Characterisation of cell cycle checkpoint kinases in *Toxoplasma gondii*

Monique K. Johnson[1], Sara Chelaghma[2], William H. Lewis[2], Ludek Koreny[2], Ross F. Waller[2], Catherine J. Merrick[1#]

[1] Department of Pathology, University of Cambridge, Tennis Court Road, Cambridge, CB2 1QP, UK.

[2] Department of Biochemistry, University of Cambridge, Tennis Court Road, Cambridge, CB2 1QW, UK.

Address correspondence to:

Department of Pathology, Cambridge University, Tennis Court Road, Cambridge, CB2 1QP, UK

Tel: (+44) 1223 333330

Email: cjm48@cam.ac.uk

ABSTRACT

Toxoplasma gondii is a protozoan parasite in the apicomplexan phylum. Apicomplexan parasites replicate using a variety of non-canonical cell division modes, distinct from binary fission, whose molecular regulation is incompletely understood. *T. gondii* replicates by endodyogeny in its intermediate hosts, and by endopolygeny in its definitive host. To improve our understanding of how these unusual, flexible cell division modes are regulated, we characterised the *T. gondii* homologues of the cell-cycle checkpoint kinases ATM and ATR. These phosphoinositol-3-kinase-like kinases are entirely absent in some related parasites including *Plasmodium*; in *T. gondii* they are present but their putative checkpoint roles were previously uncharacterised. Both *Tg*ATM and *Tg*ATR were found to be dispersed throughout the parasite, rather than restricted to the nucleus, and they did not detectably relocate to the nucleus after DNA damage. Nevertheless, they were both required for checkpoint responses to DNA damage, including acute replication slowing and phosphorylation of the DNA damage marker histone H2AX. Unusually, the two kinases seemed to

cooperate in the checkpoint response, with the loss of either one largely ablating the response, regardless of the type of DNA damage. Thus, *T. gondii* clearly retains a DNA-damage-responsive checkpoint, but some of its key features differ from the well-studied checkpoint in human cells.

AUTHOR SUMMARY

Toxoplasma is one of the most widespread parasites of humans, with a large proportion of the global population being infected. Infection usually causes no symptoms, but can have severe consequences in pregnant women and immunocompromised people. The *Toxoplasma* parasite is a single-celled organism, related to other parasites that cause important human diseases like malaria. All these parasites are distinctive in having unusual modes of replication: unlike human cells, they do not replicate by simply splitting in two. Furthermore, drugs to treat toxoplasmosis usually act to suppress the parasite's replication. Therefore, it is important to understand how this unusual replication is controlled, both for our fundamental understanding of cell division modes, and to ensure effective drug treatment of toxoplasmosis. Here, we characterised for the first time the proteins that control the *Toxoplasma* cell cycle by responding to DNA damage. We report that a damage-responsive checkpoint exists, but has some unusual features.

KEYWORDS

Toxoplasma, cell cycle, checkpoint, ATM, ATR, PIKK

INTRODUCTION

The apicomplexan parasite *Toxoplasma gondii* is a significant cause of disease in both animals and humans. It is widespread in the global human population as a largely asymptomatic infection, but it can cause lethal disease in immunocompromised patients, retinal scarring and blindness in immunocompetent individuals, and severe birth defects if pregnant women are acutely infected. Accordingly, effective drugs are required to treat acute toxoplasmosis, and concerns have recently been raised about resistance to current therapies [1]. These therapies usually consist of anti-folate

50 regimes such as pyrimethamine/sulfadiazine [2], which act to suppress folate metabolism, starve the
51 parasite of nucleotide precursors and suppress its replication. A detailed understanding of the
52 parasite's mode of replication is therefore important – both to understand the action of anti-
53 parasite drugs, and also because *Toxoplasma* replication is fundamentally unusual. As such, it can
54 illuminate our understanding of the basic biology of eukaryotic cell division.

55 *Toxoplasma* lies in the apicomplexan phylum of protozoan parasites and a key feature of this
56 deeply-diverging phylum is that the species therein do not replicate by conventional binary fission –
57 the cell division mode used by most model cells from *S. cerevisiae* to human. Instead, they employ a
58 variety of syncytial division modes, such as endodyogeny in *Toxoplasma*, endopolygeny in
59 *Sarcocystis* and schizogony in the malaria parasite *Plasmodium* [3, 4]. Many of the regulatory
60 proteins that drive and control the *Toxoplasma* cell cycle are now being identified [5-9], and some
61 elements of this cell cycle are clearly unusual, such as the apparent separation between the nuclear
62 division and budding cycles [10, 11], but comparatively little is known about stress-responsive
63 checkpoints within this cycle.

64 Eukaryotic cells make highly conserved 'checkpoint' responses to DNA damage or stalled
65 replication, involving a kinase cascade that arrests the cell cycle and promotes DNA repair [12]. This
66 is initiated by one or more members of the phosphoinositol-3-kinase-like kinase (PIKK) family. These
67 kinases – Mitosis entry checkpoint 1 (Mec1) in budding yeast; Ataxia-Telangiectasia Mutated or
68 Rad3-Related (ATM and ATR) in humans – have a catalytic domain that is structurally related to PI3K
69 lipid kinases [13]. However, they act upon protein substrates instead, including the checkpoint-
70 transducing kinases Rad53/Chk1/Chk2 and the histone H2AX, which marks damaged DNA for repair.

71 As an obligate intracellular parasite, *Toxoplasma* can certainly suffer DNA damage through
72 inflammatory stress, oxidative and free-radical damage, etc. Like most eukaryotes, it encodes
73 pathways to repair DNA double-strand breaks (DSBs): homologous recombination and non-
74 homologous end-joining [14]. Therefore, it would make evolutionary sense to retain DNA-damage-

75 responsive checkpoints. Curiously, these may be absent in at least some apicomplexans:
76 *Plasmodium* species seem to entirely lack PIKK kinases [15], and may not arrest their cycle after
77 aberrant genome replication [16, 17]. *Toxoplasma*, by contrast, does encode PIKK homologues,
78 although the downstream kinases Chk1/2 have not been clearly identified and their DNA damage
79 checkpoint has not been thoroughly investigated, despite its potential importance as a target for
80 anti-parasite drugs [18].

81 Here, we characterised for the first time the two PIKKs in *T. gondii*, which are annotated
82 *Tg*ATM and *Tg*ATR, according to their homology with human ATM and ATR. Both genes were
83 categorised as 'fitness conferring' in a Crispr-based gene knockout screen [19]. To our knowledge,
84 *Tg*ATR was entirely unstudied, while *Tg*ATM was first identified in 2010 [20] in a study of the
85 acetyltransferase *Tg*MYST. This found that *Tg*MYST may induce a putative ATM homologue, *Tg*ATM,
86 and also inferred that this homologue may phosphorylate *Tg*H2AX, although *Tg*ATM was not
87 knocked down or isolated to show this directly. A slow-growth phenotype when *Tg*MYST was over-
88 expressed was taken to represent *Tg*ATM-induced checkpoint activity, and this was ablated by an
89 inhibitor of human ATM, KU-55933, which was assumed (but not directly shown) to inhibit *Tg*ATM as
90 well. A subsequent study also used this inhibitor and showed that KU-55933 itself could slow *T.*
91 *gondii* growth, and also abolish H2AX phosphorylation after DNA damage [21].

92 Hence, there was circumstantial evidence that *Tg*ATM acts as DNA damage checkpoint
93 kinase, and could be essential for replication by endodyogeny, but neither *Tg*ATM nor *Tg*ATR had
94 been genetically manipulated or studied directly. Here, we report that *Tg*ATM and *Tg*ATR can both
95 be knocked down without any fitness defect in cultured parasites, but that both proteins – in a
96 largely overlapping manner – do enforce a DNA damage checkpoint in *T. gondii.*

97 **RESULTS**

98 <u>*T. gondii* encodes homologues of cell cycle checkpoint kinases</u>

99 To verify the presence of ATM and ATR orthologues in *T. gondii*, we performed a phylogenetic
100 analysis of known ATM/ATR proteins and their closest matches in *T. gondii* and throughout
101 apicomplexans and other major eukaryotic lineages (Figure 1, S1). This analysis also included the
102 related TOR proteins and the PI3K/PI4K kinases, which formed an outgroup. We identified single *T.*
103 *gondii* homologues of ATM, ATR and TOR, each of which was most closely related to the respective
104 human homologue. The *T. gondii* homologues of ATM, ATR and TOR were all annotated in ToxoDB
105 as putative forms of these three proteins; the single homologues of the lipid kinases PI3K and PI4K
106 were annotated in ToxoDB only as 'PI3/4 kinases' but one gene clearly grouped with PI3Ks, and the
107 other gene with PI4Ks, from both human and *Plasmodium* species.

108 The *T. gondii* proteins each grouped, with strong support, with those of other apicomplexans
109 and further related myzozoans, indicating that each of these molecules were present in the common
110 ancestor of all apicomplexans. Conspicuously, *Plasmodium* spp. lacked orthologues for ATM, ATR or
111 TOR, with the nearest orthologues found as outgroups to these PIKKs, i.e. PI3K and PI4K (Figure 1).
112 Similarly, there was independent loss of ATM from *Cryptosporidium* and the piroplasms *Babesia* and
113 *Theileria*. Thus, while both ATM and ATR occur in *T. gondii*, there is an apparent trend towards loss
114 or shift of function of these molecules in Apicomplexa.

115 In the PIKK family, ATM in human cells responds primarily to DNA DSBs, while ATR responds
116 primarily to stalled replication forks [22]. TOR has a different cell-cycle role, regulating cell growth
117 and protein production. Therefore, in *T. gondii*, homology would suggest that *Tg*ATM and *Tg*ATR
118 should be most directly involved in DNA-damage checkpoint responses to DNA DSBs and stalled
119 replication forks respectively. However, neither protein had yet been investigated, localised in the
120 parasite cell, characterised for kinase activity, or knocked out to determine essentiality.

121 <u>Inducible knockdown of *Tg*ATM and *Tg*ATR</u>

122 PIKKs are very large proteins: *Tg*ATM has a predicted size of ~250kDa, and *Tg*ATR, ~650kDa. Cloning
123 for overexpression or recombinant expression would be prohibitively difficult, as would biochemical

124 purification of these proteins. We therefore addressed the function of *Tg*ATM and *Tg*ATR by making
125 inducible knockdowns, since a genome-wide screen for essential genes in *T. gondii* had previously
126 suggested that both genes may be refractory to complete knockout [19] (Figure S2A, B).

127 The strategy for gene tagging and inducible knockdown is shown in Figure 2A and B: 5'
128 integration of a haemagglutinin (3xHA) tag and a tetracycline-repressible promoter [23, 24]. PCR
129 genotyping of the resultant mutants confirmed correct integration (Figure S2C, D). Upon induction
130 of knockdown with anhydrotetracycline (ATc), western blotting showed that all detectable HA-
131 tagged *Tg*ATM was lost within 24h and this depletion was stable through 72h (Figure S2E). A similar
132 assessment of the *Tg*ATR knockdown was not possible because the protein was too large for
133 effective western blotting. However, immunofluorescence assays (IFA) showed the near-total loss of
134 both proteins within 24h (Figure 2C, D) and this was confirmed by quantifying the
135 immunofluorescent signals. Residual fluorescence after knockdown was similar to the levels seen in
136 parental cells without any HA-tagged protein (Figure 2E, F).

137 Human ATM and ATR have a primarily nuclear location, consistent with their function [25].
138 Interestingly, however, the reporter-tagged forms of both *Tg*ATM and *Tg*ATR were detected
139 throughout the cell (Figure 2C, D), their diffuse appearance was inconsistent with localisation to any
140 subcellular organelle and confocal microscopy did not reveal further details beyond this generally
141 diffuse location. It is notable that *Tg*MYST, which has been proposed to acetylate *Tg*ATM, was also
142 reported to be cytoplasmic, contrary to its expected nuclear location [20]. Neither *Tg*ATM nor
143 *Tg*ATR appeared in the published subcellular atlas of the *Toxoplasma* proteome [23], and the
144 difficulty of handling such large, unstable proteins precluded subcellular fractionation for western
145 blotting to conclusively determine the proportions of *Tg*ATM and *Tg*ATR in nuclear and cytoplasmic
146 fractions.

147 <u>Knockdown of *Tg*ATM or *Tg*ATR imposes no growth defect or DNA-damage-sensitivity in culture</u>

148 Contrary to predictions from the genome-wide screen [19], neither gene knockdown showed an
149 overt growth phenotype in triplicate plaque assays (Figure 3A, B). We therefore concluded that
150 *Tg*ATM and *Tg*ATR were either entirely dispensable for parasite growth in normal culture conditions,
151 or that these proteins were essential but that residual protein after knockdown, albeit undetectable
152 via western blot or immunofluorescence, could suffice under normal conditions. In either case,
153 challenging the parasites with DNA damage might reveal an effect on parasite growth. Therefore,
154 parasites were subjected to two DNA damaging agents, the alkylating agent methyl methane
155 sulphonate (MMS) or the topoisomerase inhibitor camptothecin (CPT) (previously validated to cause
156 H2AX phosphorylation in this system [21]).

157 Both agents caused a titratable defect in parasite growth, the nature of which appeared to
158 be different for MMS versus CPT. MMS primarily reduced the number of plaques, suggesting acute
159 parasite killing followed by a rapid decay of its alkylating activity, so that surviving parasites grew
160 quite normally over the subsequent 10 days. CPT reduced the number but also, primarily, the size of
161 plaques that grew after 10 days, suggesting ongoing growth-inhibitory activity as well. However,
162 none of these effects was clearly exacerbated by the knockdown of either PIKK (Figure 3C-F).

163 <u>Knockdown of *Tg*ATM or *Tg*ATR ablates acute checkpoint-like responses to DNA damage</u>

164 We then reasoned that long-term growth assays might not be a suitable read-out if the knockdowns
165 did, in fact, impede a DNA damage checkpoint. Parasites that failed to respond to DNA damage and
166 continued to replicate, rather than inducing DNA repair, might initially have a growth advantage but
167 might eventually die if their genome was irreparably damaged. Hence the outcome of a 10-day
168 plaque assay might appear similar whether a checkpoint was induced or not. Accordingly, we sought
169 more acute phenotypes in the knockdown parasites.

170 A 24h 'replication assay' quantifies parasite growth during just the first ~3 cycles of
171 endodyogeny after invasion, by counting the numbers of parasites in newly formed vacuoles in
172 individual host cells (Figure 4A). Notably, this does not establish whether the cells have all arrested

173 in a particular stage – pre-replication ('G1') or during S-phase – but simply tests for an acute slowing
174 of their overall cycling rate. This assay confirmed that replication rates were indeed normal in both
175 knockdown lines. DNA damage induced by either MMS or CPT could reduce the initial replication
176 rate and the knockdown of either PIKK ablated this (Figure 4B, C), implying that cell-cycle slowing
177 after DNA damage was indeed the result of checkpoint induction, and that knockdown parasites
178 failed to induce such a checkpoint. There was little difference between the *Tg*ATM and *Tg*ATR
179 knockdowns, suggesting substantial cooperation between the two proteins, with both being similarly
180 required for an effective checkpoint response to two types of DNA damage: alkylation or
181 topoisomerase inhibition. Of note, however,the *Tg*ATM knockdown only partially restored
182 replication to normal rates after CPT damage, but did fully restore it after MMS damage at 25μM,
183 and almost fully after 50μM, while the *Tg*ATR knockdown only partially restored replication to
184 normal rates after MMS damage, but did fully restore it after CPT damage. This suggests that there is
185 some degree of specialisation between the two proteins according to different types of DNA
186 damage, but both proteins were clearly required for a fully effective response.

187 We then measured a second acute read-out for the DNA damage checkpoint:
188 phosphorylation of histone H2AX. Foci of γH2AX appeared at substantial levels in normally
189 replicating parasites, as previously reported [26-28], suggesting a high endogenous level of
190 replication stress in cultured tachyzoites. Phosphorylation appeared to be induced even further by
191 DNA damage, particularly via CPT, with brighter and larger foci of γH2AX appearing (Figure 4D, E).
192 Both the individual knockdowns ablated the γH2AX signal almost entirely, and it could not be
193 induced even after DNA damage (Figure 4F). Again, both proteins were apparently required, since
194 either one of the individual knockdown affected H2AX phosphorylation equally severely.

195 <u>*Tg*ATR does not behave quantifiably differently in the presence or absence of *Tg*ATM</u>

196 We wished to investigate the extent and nature of cooperation between *Tg*ATM and *Tg*ATR.
197 Accordingly, we added a second, distinguishable tag (3x V5) to the ATR gene in the HA-tagged,

198 inducible knockdown line for *Tg*ATM (Figure 5A). Thus, we could follow the location and quantity of
199 *Tg*ATR in cells with *Tg*ATM either present or absent (the 250-650kDa size of these proteins
200 precluding co-immunoprecipitation and western blotting to test for a direct interaction).

201 Figure 5B shows that there was no substantial colocalisation of the two proteins: both
202 appeared in speckles throughout the parasite that were largely non-overlapping. There was also no
203 clear difference, detectable by immunofluorescence, in the location or amount of *Tg*ATR in the
204 presence or absence of *Tg*ATM. The assessment of representative immunofluorescence images is
205 inherently qualitative, so we also quantified the signals in cohorts of cells: both the amount of signal
206 across individual parasites, and the maximum brightness of foci per parasite. There was
207 considerable variation in both parameters, but ATR foci did not become reproducible fainter,
208 brighter or more abundant in the absence of *Tg*ATM (Figure 5C, D). Therefore, although the two
209 proteins were required in concert to induce checkpoint phenotypes (Figure 4), we could not detect
210 any direct interaction between them. Finally, we checked whether the distribution of either protein
211 changed after DNA damage, specifically to concentrate in the nucleus, as might be expected if a DNA
212 damage response was required there. When the proportion of signal in the nucleus versus
213 cytoplasm was quantified in cohorts of cells before or after DNA damage, no clear differences were
214 seen (Figure 5E, F).

215 <u>A specific inhibitor of human ATM does not phenocopy the knockdown of *Tg*ATM or *Tg*ATR</u>

216 Previous publications used the human ATM inhibitor KU-55933 on the assumption that it would be
217 equally specific for *Tg*ATM [20, 21]. We tested this by comparing the effect of KU-55933 with the
218 effect of knocking down *Tg*ATM. Figure 6A-C shows that the KU-55933 inhibitor caused a dose-
219 dependent growth defect in a 10-day plaque assay, in contrast with either individual knockdown,
220 which did not (Figure 3). Furthermore, the growth defect imposed by the inhibitor was similar
221 whether an individual PIKK was also knocked down or not (Figure 6C). This led to two potential
222 conclusions: either the effect of KU-55933 was 'off target' (via a pathway unrelated to

223 *Tg*ATM/*Tg*ATR), or alternatively, the inhibitor was targeting both PIKKs and this complete loss of
224 function was more deleterious for *T. gondii* than the loss of either one alone.

225 We checked whether treatment with KU-55933 could affect either the amount of *Tg*ATM or
226 *Tg*ATR in individual parasites, or the maximum brightness of their foci per parasite, by quantifying
227 IFA images as in figure 5. No consistent changes were detected in the foci of either protein (except,
228 as expected, when *Tg*ATM was knocked down) (Figure 6D). However, when the total quantity of
229 protein per parasite was measured, KU-55933 treatment did correlate with an overall increase in the
230 amount of *Tg*ATM, whereas there was no change in *Tg*ATR (Figure 6E). This implied that KU-55933
231 might indeed inhibit *Tg*ATM (and potentially also *Tg*ATR) and that the parasite might respond to this
232 by upregulating *Tg*ATM expression.

233 To further distinguish between the possibilities of off-target killing or pan-PIKK inhibition, we
234 checked the previously published result that cells treated with KU-55933 could not phosphorylate
235 H2AX [21]. This was confirmed: the inhibitor largely prevented γH2AX foci from forming, both in
236 endogenous replication and in response to DNA damage (Figure 6F). In this regard, inhibitor-
237 treatment was similar to the individual knockdown of *Tg*ATM (or *Tg*ATR). Since KU-55933 inhibits
238 human ATM as well, H2AX phosphorylation was equally inhibited in the human host cell nuclei, as
239 expected (Figure S3). Overall, it appeared likely that KU-55933 did in fact inhibit *Tg*ATM, but that it
240 additionally affected *Tg*ATR and/or other off-target proteins, resulting in a growth defect.

241 **DISCUSSION**

242 This work characterised the two PIKK homologues in *Toxoplasma gondii*, with the aim of establishing
243 whether or not they act as DNA damage checkpoint kinases. This was an important question
244 because toxoplasmosis is often treated with drugs that may cause DNA damage, and also because it
245 could help to establish how damage-responsive checkpoints have evolved across the apicomplexan
246 phylum. In this large phylum of early-diverging protists, some parasites, like *T. gondii*, retain PIKK
247 homologue(s) while other important parasites, like *Plasmodium* spp., appear to have lost them.

248 We established, phylogenetically, that *T. gondii* does encode orthologues of all the classes of
249 PIKKs defined in human cells. We then tagged and knocked down the orthologues of ATM and ATR.
250 The first striking observation was that neither protein was primarily nuclear, but appeared diffusely
251 throughout the cytoplasm, in largely non-overlapping speckles that were inconsistent with any
252 particular organelle. It is notable that another protein with a predicted nuclear role, the
253 acetyltransferase *Tg*MYST, was also reported thus [20], and proposed to shuttle to the nucleus. In
254 human cells, although ATM is nuclear, it can under some stimuli shuttle to the cytoplasm [29]. We,
255 however, found no clear evidence that either *Tg*ATM or *Tg*ATR shuttled between cytoplasm and
256 nucleus after DNA damage.

257 Both *Tg*ATM and *Tg*ATR were then inducibly knocked down, with near-100% efficiency as
258 seen by immunofluorescence, and also by western blotting in the case of *Tg*ATM. As with any
259 inducible gene regulation, some residual protein might remain. However, under severe-knockdown
260 conditions, we found no evidence that either protein was essential or had any effect on normal cell
261 growth. Nevertheless, after DNA damage, both knockdowns did ablate an acute reduction in cellular
262 replication, as well as another key marker of the DNA damage response: phosphorylation of histone
263 H2AX, which showed that a genuine kinase-driven checkpoint signal occurred, and that this required
264 *Tg*ATM/*Tg*ATR. Thus, there was strong evidence for a canonical checkpoint role for these proteins.
265 This was not initially detected in plaque assays simply because these assays occur over 10 days and
266 many lytic cycles. Any parasites that failed to respond to DNA damage and continued to replicate
267 would probably die from irreparable genome damage before a large plaque could be formed,
268 resulting in a similar outcome to that seen in parasites that sustained damage and did make a
269 checkpoint response, arresting or slowing their growth.

270 Our study did not address whether the DNA damage checkpoint in *T. gondii* is enforced
271 equally in all phases of the cell cycle. In human cells, damage such as DSBs can be detected and
272 repaired in G1 and G2 as well as S-phase, whereas other types of damage can be replication-

273 dependent – detected efficiently only when replication forks are active during S-phase. Further
274 dissection of this issue would require clear phase markers in *T. gondii:* for example, cells in S-phase
275 might be detected by bromodeoxyuridine labelling of nascent DNA or fluorescent labelling of
276 proliferating cell nuclear antigen (PCNA). These have both been achieved in *Plasmodium* [30, 31],
277 but have yet to be demonstrated in *Toxoplasma.*

278 In human cells, ATR responds primarily to stalled replication forks and ATM, to DNA DSBs
279 [32]. To establish whether *Tg*ATM and *Tg*ATR acted similarly, we used two different DNA damaging
280 agents, the alkylating agent MMS, well-established to cause fork stalling at alkylated bases, and the
281 topoisomerase inhibitor CPT, which can induce DNA breaks. (Of note, our knockdowns were made
282 in a background deficient for non-homologous end-joining, but still competent to repair DSBs by
283 homologous recombination.) Interestingly, we detected little 'division of labour' between *Tg*ATM
284 and *Tg*ATR: the phenotypes in H2AX phosphorylation and cellular replication were similarly affected
285 by both knockdowns. The only detectable difference was that high concentrations of MMS still
286 elicited some replication-slowing when *Tg*ATR was lost, but not when *Tg*ATM was lost, and the
287 converse was true of CPT, suggesting that *Tg*ATM may be more important in responding to alkylation
288 damage and *Tg*ATR, to DNA breakage. This would be the opposite specialisation of protein function
289 to that in human cells. Generally, however, both proteins were required to induce both types of
290 DNA-damage checkpoint.

291 Despite this, we found no evidence for their colocalization or reciprocal up/down-regulation,
292 so it is unlikely that the two proteins act in a stable complex. Mutual regulation, such as
293 transphosphorylation, may be more likely. In human cells, ATM exists as an inactive dimer and is
294 induced to autophosphorylate after DNA damage, whereupon it dissociates and its monomers act on
295 downstream substrates [33]. Perhaps in *T. gondii*, activating phosphorylation event(s) occur
296 primarily *in trans* and require both PIKKs, or perhaps both PIKKs act in mutually-essential ways on a
297 single transducer downstream. (In humans, ATM and ATR activate Chk2 and Chk1 respectively [32],

298 but neither of the Chk kinases has been identified in *T.gondii*). Biochemical experiments would be
299 required to interrogate these hypotheses, such as generating complete phosphoproteomes of
300 knockdown parasites, or co-immunoprecipitating the PIKKs to seek evidence for their cross-
301 phosphorylation. With proteins of 250-650kDa, and of low abundance (neither was detected in the
302 subcellular atlas of the *Toxoplasma* proteome [24]), such assays are non-trivial.

303 We attempted to further separate the activities of the two proteins using a 'specific' small-
304 molecule inhibitor of human ATM, KU-55933, but this did not phenocopy the *Tg*ATM knockdown.
305 The inhibitor severely affected cell growth, suggesting either off-target effects or an equal inhibition
306 of both PIKKs, with this being more deleterious than either single knockdown. Since the inhibitor
307 ablated H2AX phosphorylation, and had the same effect with or without either genetic knockdown,
308 we favoured the latter explanation. Although we were unable to generate a double genetic
309 knockdown, KU-55933 may itself generate this effect. If so, this implies that the complete loss of all
310 PIKK activity does affect cell growth and viability. This would be expected, since DNA damage occurs
311 during normal replication (as marked by γH2AX), and constant checkpoint activation is probably
312 required in replicating tachyzoites. Curiously, *Tg*ATM and *Tg*ATR seem to be mutually required for
313 this, but perhaps in each genetic knockdown, the single remaining protein achieves some level of
314 self-activation (or a very low residual level of either knocked-down protein can transphosphorylate
315 the other), thus yielding a low-level response and hence cell survival, whereas KU-55933-treated
316 cells make no response at all.

317 Overall, we conclude that *T. gondii* does have PIKK kinases that enforce a DNA-damage
318 checkpoint, slowing down cellular replication and phosphorylating the DNA damage marker H2AX.
319 Unusually, both *Tg*ATM and *Tg*ATR seem to be required for this, regardless of the type of DNA
320 damage. This could represent a step towards the tendency for reductive evolution of PIKKs in
321 apicomplexans: ATR is found broadly, although lost from *Plasmodium* spp., whereas ATM is
322 independently lost from *Cryptosporidium*, *Babesia* and *Theileria* (Figure 1). This might, in turn, help

323 to explain the apparently-unique situation in *Plasmodium*, where both PIKK homologues are entirely
324 lost. (Whether checkpoint activity is then lost in *Plasmodium*, or transferred to another protein,
325 remains to be explored.)

326 In terms of cell division, apicomplexan parasites are particularly interesting because they can
327 divide by different modes at different lifecycle stages. For example, *Plasmodium* uses schizogony in
328 the blood stage and something resembling endopolygeny in the oocyst [34]; *T. gondii* uses
329 endodyogeny in intermediate hosts and a division mode that is variously defined in the literature as
330 endopolygeny or schizogony in the definitive feline host [35-38]. Whether DNA damage checkpoints
331 are equally active in both stages cannot presently be investigated, because experimental access to
332 the feline stage in *T. gondii* is very limited. Nevertheless, further investigation of cell-cycle
333 checkpoints in *T. gondii* might usefully inform the study of checkpoints in other apicomplexans such
334 as *Plasmodium* as well.

335

336 **METHODS**

337 Database sampling and phylogenetic analysis

338 A custom database was collated that included data for relevant eukaryote species from UniProt [39]
339 and the Marine Microbial Eukaryote Transcriptome Sequencing Project [40], as well as data for
340 apicomplexans and close relatives from VEuPathDB [41] and two previous studies [42, 43]. This
341 custom database was then sampled for ATM, ATR and TOR homologues using the program blastp
342 (BLAST+ version 2.11.0 [44]), for which characterised homologues of these proteins from selected
343 model organisms, including *T. gondii*, were used as search queries. The dataset of possible ATM, ATR
344 and TOR homologues obtained was then clustered with CD-HIT [45] to remove highly similar
345 sequences, thereby reducing overall redundancy of the dataset. Iterative rounds of alignment were
346 then performed using mafft (MAFFT version 7.475 [46]), conserved site selection using trimal with
347 "gappyout" mode (trimAl version 1.4 [47]), and tree inference with FastTreeMP (FastTree version

348 2.1.11 [48]) using the default settings and manual removal of sequences to further reduce dataset
349 redundancy. Manual removal also identified and removed sequences that aligned poorly or were so
350 dissimilar from the majority of the sequences in the dataset that they were unlikely to be ATM, ATR
351 or TOR homologues, but rather false positives of the described sampling strategy. The final curated
352 dataset that these methods obtained was then aligned using mafft-linsi (MAFFT version 7.475 [46])
353 and conserved sites were selected using trimal with "gappyout" mode (trimAl version 1.4 [47]). A
354 phylogeny was then inferred from this dataset using the program iqtree2 (IQ-TREE version 2.1.2
355 [49]) with 1000 ultrafast bootstrap replicates (UFBoot2 [50]) and using the best-fitting model,
356 LG+F+I+G4 ([51]) that was chosen according to the Bayesian Information Criterion by ModelFinder
357 [52], all implemented within iqtree2. The protein sequences, alignment, and tree inference output
358 files used to generate the phylogeny are provided at [Journal preferred repository?].

359 Parasite strains and growth

360 *Toxoplasma gondii* (*T. gondii*) tachyzoites from the strain RH and derived strains, including
361 Δ*ku80*:TATi tachyzoites (a gift from Lilach Sheiner and Boris Striepen, University of Georgia) [53],
362 were grown on a confluent monolayer of human foreskin fibroblast (HFF) cells in 10 ml flasks of ED1
363 (Dulbecco's Modified Eagles Medium supplemented with 1% foetal bovine serum (FBS), 0.2 mM L-
364 glutamine, 0.25 µg ml^{-1} Fungizone (ThermoFisher), 10 unit ml^{-1} penicillin and 10 µg ml^{-1} streptomycin
365 (ThermoFisher)) and maintained at 37 °C with 10% CO_2, as previously described [54].

366 Creation of transgenic *T. gondii*

367 Gene tagging was performed as described by Waller and colleagues [23]. A CRISPR/Cas9-assisted,
368 PCR-mediated tagging strategy was used to perform endogenous gene tagging with epitope tags
369 and/or endogenous promoter replacement with an ATc-regulatable t7s4 promoter. The generation
370 of transgenic *T. gondii* involved a level M Cas9/sgRNA plasmid, P5, containing a specific protospacer
371 sequence for directing a locus-specific DNA break to facilitate homologous recombination-driven
372 insertion of the donor DNA fragment. Protospacer sequences were designed for insertion into the
373 N-terminus of genes encoding putative *T. gondii* homologues of ATR (TGGT1_283702) and ATM

374 (TGGT1_248530) (Figure S4). The donor DNA fragment was PCR amplified from one of the template
375 plasmid vectors (Figure S4A) using primers (Figure S4B) that included specific homology arms
376 directing the integration of this donor DNA construct into the target genetic locus for ATM and ATR.
377 Electroporation of these constructs was completed as in [23].

378 Parasite genomic DNA extraction for PCR confirmation

379 T25 flasks containing mostly extracellular *T. gondii* were scraped and host cell debris was pelleted at
380 100 *xg* for 5 min. A 1-1.5 ml aliquot was harvested from the supernatant, containing 0.5-5 x 10^6 fully
381 lysed *T. gondii* tachyzoites, and these were collected by centrifugation (7,000 *xg*/full speed, 2 min).
382 The cell pellet was resuspended in 20 µl proteinase K solution: 5% proteinase K (Thermo Scientific,
383 EO0491), 10% PCR buffer 10x (Roche, 11732650001), 85% dH_2O. This was incubated at 45 °C for 60
384 min. The proteinase was heat inactivated at 94 °C for 10 min. The remaining solution was used to
385 run PCR directly, 0.3 - 1.5 µl as DNA template for a 20 µl PCR reaction.

386 Plaque assay

387 Plaque assays required parasites derived from freshly lysed host cells, which were centrifuged at 100
388 *xg* for 5 min to remove host cell debris. The same number of parasites (around 500) was added to
389 each new T25 flask containing HFF monolayer. In experiments testing the knockdown (k/d) of a
390 target gene, a control of untreated *T. gondii* infected HFFs was used, as well as ATc-treated (k/d) *T.*
391 *gondii* infected HFFs. For the ATc treatment, 0.5 µg/ml of ATc was added. After 10 days of
392 incubation at 37 °C and with 10% CO_2, the media from flasks was aspirated and the cells were
393 washed once with PBS. Cells were fixed with 5 ml of 100% ice-cold methanol for 5 min and stained
394 with 5 ml of 1% crystal violet solution for 15 min. After staining, crystal violet solution was removed
395 and flasks were washed three times with PBS. Flasks were allowed to dry, then imaged for
396 qualitative analysis. Quantitative analysis was also performed on representative fields from three
397 biological replicates, calculating the percentage plaque area in each field of host cells via ImageJ.

398 Immunofluorescence

399 *T.gondii* infected HFFs were grown on glass coverslips in 6 well plates. Cells were fixed to coverslips
400 with 2% PFA/PBS for 15 min at RT and permeabilised with 0.02% TritonX100 in PBS for 10 min. Cells
401 were blocked for 1 h in 2% BSA/PBS. Coverslips were incubated with primary antibody in blocking
402 solution for 1 h and then incubated in secondary antibodies in 2% BSA/PBS for 1 h in the dark. 120
403 µl of 2 µg/ml DAPI solution (Merck) was added for 10 min and then coverslips were mounted on
404 slides in ProLong® Diamond Antifade (ThermoFisher, P36961). Images were acquired using a Nikon
405 Eclipse Ti widefield microscope with a Nikon objective lens (Plan APO, 100x/1.45 oil), and a
406 Hamamatsu C11440, ORCA Flash 4.0 camera. Images were processed using the NIS-Elements
407 software and ImageJ (v.1.51w).

408 Replication assay

409 For the replication assay parasites were pre-treated with or without ATc for 48 h. Parasites derived
410 from freshly lysed host cells were counted and an equal number (1.6×10^6) was added to HFF
411 monolayers grown on coverslips in 6-well plates. Cells were incubated for 2 h at 37 °C to allow
412 invasion. Parasites that had not invaded were washed off three times with warm ED1. Parasites
413 were then exposed to the DNA damaging agents CPT or MMS, allowed to grow for a further 24 h
414 (still with or without ATc), then fixed as per the protocol for immunofluorescence and mounted onto
415 slides using DAPI stain only. Images were acquired using a Nikon Eclipse Ti widefield microscope with
416 a Nikon objective lens (Plan APO, 100x/1.45 oil), and a Hamamatsu C11440, ORCA Flash 4.0 camera.
417 Images were processed using the NIS-Elements software and ImageJ (v.1.51w). Numbers of
418 parasites in each vacuole were counted for 250 vacuoles per condition.

419 Immunoblotting

420 Approximately 50×10^6 parasites were purified from the host cell debris by filtration through 3-µm-
421 pore-size polycarbonate film membrane filters (Nuclepore Track-Etch Membrane, Whatman). Cells
422 were collected and washed in PBS by centrifugation at 1,700 × *g* for 10 min at RT, then pellets were
423 resuspended in 1x RIPA buffer (150 mM sodium chloride, 1.0% NP-40 or Triton X-100, 0.5% sodium

424 deoxycholate, 0.1% SDS (sodium dodecyl sulfate) and 50 mM Tris pH 8, added to 50 ml dH_20).
425 Protease inhibitors (ROCHE, cOmplete Mini) were added to 10 ml aliquots directly before use).
426 Samples were freeze-thawed 3 times by placing tubes in dry ice / 100% ethanol and a heated
427 Eppendorf block at 37 °C. Cell debris was pelleted at 4 °C at 13,000 *xg*, then supernatant was
428 removed to a new Eppendorf. 1 x NuPage LDS Sample Buffer (ThermoFisher: NP0007),
429 supplemented with 0.1% 2-mercaptoethanol, was added to samples and boiled at 90 °C for 5 min.
430 Protein lysates were resolved on SDS-PAGE in a 4-15% TRIS-glycine gel (BIO-RAD Mini -PROTEAN®
431 TGX™) together with a molecular weight marker, Page Ruler Plus (ProteinTech). Gels were run for
432 1–2 h at 100 V until the ladder 10 kDa band was at the bottom of the gel. Nitrocellulose membrane
433 0.2-µM-pore-size (Amersham™ Protran®, GE Healthcare) was cut to size and wetted in transfer
434 buffer. Wet electro-transfer was completed in transfer buffer at 60 V for 45 min.
435 Membrane was blocked with 3% BSA TBST for 1 h, washed once in TBST and incubated
436 overnight in primary antibody diluted in blocking buffer at 4 °C. The blot was washed 3x 5 min in
437 TBST and incubated in a secondary antibody diluted 1:5000 in blocking buffer for 1 h. Blots were
438 washed again 3x 5 min, TBST, developed using SuperSignal™ West Pico Plus Chemiluminescent
439 Substrate (Thermo Scientific) and imaged on the gel imager (Azure, Q500).
440 <u>IFA quantification analysis</u>
441 IFA images were analysed by creating regions of interest (ROI) encompassing single parasites, or
442 nuclei, in Image J. ROIs were created in ImageJ using the 'threshold, analyse particles' function.
443 ROIs of between 500-5000 pixels were selected; overlapping cells and top-down cells were removed
444 visually. For nuclei vs whole cell analyses, ROIs for the nuclei were made using DAPI channel images
445 and then matched to whole cell ROIs using X, Y coordinates. Mean (average signal per cell), and Max
446 (maximum signal pixel per cell) gray values were measured from each channel. One biological
447 replicate was analysed for these analyses.
448
449

450 **ACKNOWLEDGEMENTS**

451 This work was funded by the European Research Council (ERC) under the European Union's Horizon
452 2020 research and innovation programme (ERC-2016-COG 725126 to CJM); Wellcome
453 Award 214298/Z/18/Z to RFW; and a PhD studentship from the University of Cambridge Department
454 of Pathology to MJK. The funders had no role in study design, data collection, interpretation or the
455 decision to submit the work for publication.

456

457 **REFERENCES**

458 1. Montazeri M, Mehrzadi S, Sharif M, Sarvi S, Tanzifi A, Aghayan SA, et al. Drug Resistance in
459 Toxoplasma gondii. Front Microbiol. 2018;9:2587. doi: 10.3389/fmicb.2018.02587. PubMed PMID:
460 30420849; PubMed Central PMCID: PMCPMC6215853.
461 2. Neville AJ, Zach SJ, Wang X, Larson JJ, Judge AK, Davis LA, et al. Clinically Available Medicines
462 Demonstrating Anti-Toxoplasma Activity. Antimicrobial agents and chemotherapy.
463 2015;59(12):7161-9. doi: 10.1128/AAC.02009-15. PubMed PMID: 26392504; PubMed Central
464 PMCID: PMCPMC4649158.
465 3. Francia ME, Striepen B. Cell division in apicomplexan parasites. Nat Rev Microbiol.
466 2014;12(2):125-36. doi: 10.1038/nrmicro3184. PubMed PMID: 24384598.
467 4. Striepen B, Jordan CN, Reiff S, van Dooren GG. Building the perfect parasite: cell division in
468 apicomplexa. PLoS pathogens. 2007;3(6):e78. doi: 10.1371/journal.ppat.0030078. PubMed PMID:
469 17604449; PubMed Central PMCID: PMCPMC1904476.
470 5. Sinai AP, Suvorova ES. The RESTRICTION checkpoint: a window of opportunity governing
471 developmental transitions in Toxoplasma gondii. Curr Opin Microbiol. 2020;58:99-105. doi:
472 10.1016/j.mib.2020.09.009. PubMed PMID: 33065371; PubMed Central PMCID: PMCPMC8019522.
473 6. Hawkins LM, Naumov AV, Batra M, Wang C, Chaput D, Suvorova ES. Novel CRK-Cyclin
474 Complex Controls Spindle Assembly Checkpoint in Toxoplasma Endodyogeny. mBio.
475 2021;13(1):e0356121. doi: 10.1128/mbio.03561-21. PubMed PMID: 35130726; PubMed Central
476 PMCID: PMCPMC8822342.
477 7. Alvarez CA, Suvorova ES. Checkpoints of apicomplexan cell division identified in Toxoplasma
478 gondii. PLoS pathogens. 2017;13(7):e1006483. doi: 10.1371/journal.ppat.1006483. PubMed PMID:
479 28671988; PubMed Central PMCID: PMCPMC5510908.
480 8. Suvorova ES, Francia M, Striepen B, White MW. A novel bipartite centrosome coordinates
481 the apicomplexan cell cycle. PLoS biology. 2015;13(3):e1002093. doi: 10.1371/journal.pbio.1002093.
482 PubMed PMID: 25734885; PubMed Central PMCID: PMC4348508.
483 9. Gubbels MJ, Coppens I, Zarringhalam K, Duraisingh MT, Engelberg K. The Modular Circuitry
484 of Apicomplexan Cell Division Plasticity. Front Cell Infect Microbiol. 2021;11:670049. doi:
485 10.3389/fcimb.2021.670049. PubMed PMID: 33912479; PubMed Central PMCID: PMCPMC8072463.
486 10. Tomasina R, Gonzalez FC, Martins-Duarte ES, Bastin P, Gissot M, Francia ME. Separate To
487 Operate: the Centriole-Free Inner Core of the Centrosome Regulates the Assembly of the
488 Intranuclear Spindle in Toxoplasma gondii. mBio. 2022;13(5):e0185922. doi: 10.1128/mbio.01859-
489 22. PubMed PMID: 36069445; PubMed Central PMCID: PMCPMC9600614.
490 11. Khelifa AS, Bhaskaran M, Boissavy T, Mouveaux T, Silva TA, Chhuon C, et al. PP1 phosphatase
491 controls both daughter cell formation and amylopectin levels in Toxoplasma gondii. PLoS biology.

492 2024;22(9):e3002791. doi: 10.1371/journal.pbio.3002791. PubMed PMID: 39255306; PubMed
493 Central PMCID: PMCPMC11414933.
494 12. Zhou BB, Elledge SJ. The DNA damage response: putting checkpoints in perspective. Nature.
495 2000;408(6811):433-9. doi: 10.1038/35044005. PubMed PMID: 11100718.
496 13. Perry J, Kleckner N. The ATRs, ATMs, and TORs are giant HEAT repeat proteins. Cell.
497 2003;112(2):151-5. doi: 10.1016/s0092-8674(03)00033-3. PubMed PMID: 12553904.
498 14. Fenoy IM, Bogado SS, Contreras SM, Gottifredi V, Angel SO. The Knowns Unknowns:
499 Exploring the Homologous Recombination Repair Pathway in Toxoplasma gondii. Front Microbiol.
500 2016;7:627. doi: 10.3389/fmicb.2016.00627. PubMed PMID: 27199954; PubMed Central PMCID:
501 PMCPMC4853372.
502 15. Matthews H, Duffy CW, Merrick CJ. Checks and balances? DNA replication and the cell cycle
503 in Plasmodium. Parasit Vectors. 2018;11(1):216. doi: 10.1186/s13071-018-2800-1. PubMed PMID:
504 29587837; PubMed Central PMCID: PMCPMC5872521.
505 16. Absalon S, Dvorin JD. Depletion of the mini-chromosome maintenance complex binding
506 protein allows the progression of cytokinesis despite abnormal karyokinesis during the asexual
507 development of Plasmodium falciparum. Cellular microbiology. 2021;23(3):e13284. doi:
508 10.1111/cmi.13284. PubMed PMID: 33124706; PubMed Central PMCID: PMCPMC8058698.
509 17. Matthews H, McDonald J, Totanes FIG, Merrick CJ. Dynamics of DNA replication during male
510 gametogenesis in the malaria parasite Plasmodium falciparum. Cellular microbiology. 2022. doi:
511 doi.org/10.1101/2021.12.18.473304
512 18. Angel SO, Vanagas L, Ruiz DM, Cristaldi C, Saldarriaga Cartagena AM, Sullivan WJ, Jr.
513 Emerging Therapeutic Targets Against Toxoplasma gondii: Update on DNA Repair Response
514 Inhibitors and Genotoxic Drugs. Front Cell Infect Microbiol. 2020;10:289. doi:
515 10.3389/fcimb.2020.00289. PubMed PMID: 32656097; PubMed Central PMCID: PMCPMC7325978.
516 19. Sidik SM, Huet D, Ganesan SM, Huynh MH, Wang T, Nasamu AS, et al. A Genome-wide
517 CRISPR Screen in Toxoplasma Identifies Essential Apicomplexan Genes. Cell. 2016;166(6):1423-35
518 e12. doi: 10.1016/j.cell.2016.08.019. PubMed PMID: 27594426; PubMed Central PMCID:
519 PMCPMC5017925.
520 20. Vonlaufen N, Naguleswaran A, Coppens I, Sullivan WJ, Jr. MYST family lysine
521 acetyltransferase facilitates ataxia telangiectasia mutated (ATM) kinase-mediated DNA damage
522 response in Toxoplasma gondii. The Journal of biological chemistry. 2010;285(15):11154-61. doi:
523 10.1074/jbc.M109.066134. PubMed PMID: 20159970; PubMed Central PMCID: PMCPMC2856992.
524 21. Munera Lopez J, Ganuza A, Bogado SS, Munoz D, Ruiz DM, Sullivan WJ, Jr., et al. Evaluation
525 of ATM Kinase Inhibitor KU-55933 as Potential Anti-Toxoplasma gondii Agent. Front Cell Infect
526 Microbiol. 2019;9:26. doi: 10.3389/fcimb.2019.00026. PubMed PMID: 30815397; PubMed Central
527 PMCID: PMCPMC6381018.
528 22. Helt CE, Cliby WA, Keng PC, Bambara RA, O'Reilly MA. Ataxia telangiectasia mutated (ATM)
529 and ATM and Rad3-related protein exhibit selective target specificities in response to different forms
530 of DNA damage. The Journal of biological chemistry. 2005;280(2):1186-92. doi:
531 10.1074/jbc.M410873200. PubMed PMID: 15533933.
532 23. Barylyuk K, Koreny L, Ke H, Butterworth S, Crook OM, Lassadi I, et al. A Comprehensive
533 Subcellular Atlas of the Toxoplasma Proteome via hyperLOPIT Provides Spatial Context for Protein
534 Functions. Cell host & microbe. 2020;28(5):752-66 e9. doi: 10.1016/j.chom.2020.09.011. PubMed
535 PMID: 33053376; PubMed Central PMCID: PMCPMC7670262.
536 24. Meissner M, Brecht S, Bujard H, Soldati D. Modulation of myosin A expression by a newly
537 established tetracycline repressor-based inducible system in Toxoplasma gondii. Nucleic acids
538 research. 2001;29(22):E115. doi: 10.1093/nar/29.22.e115. PubMed PMID: 11713335; PubMed
539 Central PMCID: PMCPMC92585.
540 25. Keegan KS, Holtzman DA, Plug AW, Christenson ER, Brainerd EE, Flaggs G, et al. The Atr and
541 Atm protein kinases associate with different sites along meiotically pairing chromosomes. Genes &
542 development. 1996;10(19):2423-37. doi: 10.1101/gad.10.19.2423. PubMed PMID: 8843195.

543 26. Bogado SS, Dalmasso MC, Ganuza A, Kim K, Sullivan WJ, Jr., Angel SO, et al. Canonical
544 histone H2Ba and H2A.X dimerize in an opposite genomic localization to H2A.Z/H2B.Z dimers in
545 Toxoplasma gondii. Molecular and biochemical parasitology. 2014;197(1-2):36-42. doi:
546 10.1016/j.molbiopara.2014.09.009. PubMed PMID: 25286383; PubMed Central PMCID:
547 PMCPMC4254167.
548 27. Dalmasso MC, Onyango DO, Naguleswaran A, Sullivan WJ, Jr., Angel SO. Toxoplasma H2A
549 variants reveal novel insights into nucleosome composition and functions for this histone family.
550 Journal of molecular biology. 2009;392(1):33-47. doi: 10.1016/j.jmb.2009.07.017. PubMed PMID:
551 19607843; PubMed Central PMCID: PMCPMC2734877.
552 28. Nardelli SC, Che FY, Silmon de Monerri NC, Xiao H, Nieves E, Madrid-Aliste C, et al. The
553 histone code of Toxoplasma gondii comprises conserved and unique posttranslational modifications.
554 mBio. 2013;4(6):e00922-13. doi: 10.1128/mBio.00922-13. PubMed PMID: 24327343; PubMed
555 Central PMCID: PMCPMC3870261.
556 29. Wu ZH, Shi Y, Tibbetts RS, Miyamoto S. Molecular linkage between the kinase ATM and NF-
557 kappaB signaling in response to genotoxic stimuli. Science (New York, NY. 2006;311(5764):1141-6.
558 doi: 10.1126/science.1121513. PubMed PMID: 16497931.
559 30. Merrick CJ. Transfection with thymidine kinase permits bromodeoxyuridine labelling of DNA
560 replication in the human malaria parasite Plasmodium falciparum. Malar J. 2015;14(490). doi:
561 10.1186/s12936-015-1014-7.
562 31. Klaus S, Binder P, Kim J, Machado M, Funaya C, Schaaf V, et al. Asynchronous nuclear cycles
563 in multinucleated Plasmodium falciparum facilitate rapid proliferation. Sci Adv. 2022;8(13):eabj5362.
564 doi: 10.1126/sciadv.abj5362. PubMed PMID: 35353560.
565 32. Falck J, Petrini JH, Williams BR, Lukas J, Bartek J. The DNA damage-dependent intra-S phase
566 checkpoint is regulated by parallel pathways. Nature genetics. 2002;30(3):290-4. doi:
567 10.1038/ng845. PubMed PMID: 11850621.
568 33. Bakkenist CJ, Kastan MB. DNA damage activates ATM through intermolecular
569 autophosphorylation and dimer dissociation. Nature. 2003;421(6922):499-506. doi:
570 10.1038/nature01368. PubMed PMID: 12556884.
571 34. Araki T, Kawai S, Kakuta S, Kobayashi H, Umeki Y, Saito-Nakano Y, et al. Three-dimensional
572 electron microscopy analysis reveals endopolygeny-like nuclear architecture segregation in
573 Plasmodium oocyst development. Parasitol Int. 2020;76:102034. doi: 10.1016/j.parint.2019.102034.
574 PubMed PMID: 31805442.
575 35. Gubbels MJ, Keroack CD, Dangoudoubiyam S, Worliczek HL, Paul AS, Bauwens C, et al.
576 Fussing About Fission: Defining Variety Among Mainstream and Exotic Apicomplexan Cell Division
577 Modes. Front Cell Infect Microbiol. 2020;10:269. doi: 10.3389/fcimb.2020.00269. PubMed PMID:
578 32582569; PubMed Central PMCID: PMCPMC7289922.
579 36. Hutchison WM, Dunachie JF, Siim JC, Work K. Coccidian-like nature of Toxoplasma gondii. Br
580 Med J. 1970;1(5689):142-4. doi: 10.1136/bmj.1.5689.142. PubMed PMID: 5413951; PubMed Central
581 PMCID: PMCPMC1699084.
582 37. Dubey JP, Frenkel JK. Cyst-induced toxoplasmosis in cats. J Protozool. 1972;19(1):155-77.
583 doi: 10.1111/j.1550-7408.1972.tb03431.x. PubMed PMID: 5008846.
584 38. Ferguson DJ, Hutchison WM, Dunachie JF, Siim JC. Ultrastructural study of early stages of
585 asexual multiplication and microgametogony of Toxoplasma gondii in the small intestine of the cat.
586 Acta Pathol Microbiol Scand B Microbiol Immunol. 1974;82(2):167-81. doi: 10.1111/j.1699-
587 0463.1974.tb02309.x. PubMed PMID: 4528099.
588 39. UniProt C. UniProt: the Universal Protein Knowledgebase in 2023. Nucleic acids research.
589 2023;51(D1):D523-D31. doi: 10.1093/nar/gkac1052. PubMed PMID: 36408920; PubMed Central
590 PMCID: PMCPMC9825514.
591 40. Keeling PJ, Burki F, Wilcox HM, Allam B, Allen EE, Amaral-Zettler LA, et al. The Marine
592 Microbial Eukaryote Transcriptome Sequencing Project (MMETSP): illuminating the functional
593 diversity of eukaryotic life in the oceans through transcriptome sequencing. PLoS biology.

594 2014;12(6):e1001889. doi: 10.1371/journal.pbio.1001889. PubMed PMID: 24959919; PubMed
595 Central PMCID: PMCPMC4068987.
596 41. Alvarez-Jarreta J, Amos B, Aurrecoechea C, Bah S, Barba M, Barreto A, et al. VEuPathDB: the
597 eukaryotic pathogen, vector and host bioinformatics resource center in 2023. Nucleic acids research.
598 2024;52(D1):D808-D16. doi: 10.1093/nar/gkad1003. PubMed PMID: 37953350; PubMed Central
599 PMCID: PMCPMC10767879.
600 42. Mathur V, Kolisko M, Hehenberger E, Irwin NAT, Leander BS, Kristmundsson A, et al.
601 Multiple Independent Origins of Apicomplexan-Like Parasites. Curr Biol. 2019;29(17):2936-41 e5.
602 doi: 10.1016/j.cub.2019.07.019. PubMed PMID: 31422883.
603 43. Janouskovec J, Paskerova GG, Miroliubova TS, Mikhailov KV, Birley T, Aleoshin VV, et al.
604 Apicomplexan-like parasites are polyphyletic and widely but selectively dependent on cryptic plastid
605 organelles. Elife. 2019;8. doi: 10.7554/eLife.49662. PubMed PMID: 31418692; PubMed Central
606 PMCID: PMCPMC6733595.
607 44. Camacho C, Coulouris G, Avagyan V, Ma N, Papadopoulos J, Bealer K, et al. BLAST+:
608 architecture and applications. BMC bioinformatics. 2009;10:421. doi: 10.1186/1471-2105-10-421.
609 PubMed PMID: 20003500; PubMed Central PMCID: PMCPMC2803857.
610 45. Fu L, Niu B, Zhu Z, Wu S, Li W. CD-HIT: accelerated for clustering the next-generation
611 sequencing data. Bioinformatics. 2012;28(23):3150-2. doi: 10.1093/bioinformatics/bts565. PubMed
612 PMID: 23060610; PubMed Central PMCID: PMCPMC3516142.
613 46. Katoh K, Standley DM. MAFFT multiple sequence alignment software version 7:
614 improvements in performance and usability. Mol Biol Evol. 2013;30(4):772-80. doi:
615 10.1093/molbev/mst010. PubMed PMID: 23329690; PubMed Central PMCID: PMCPMC3603318.
616 47. Capella-Gutierrez S, Silla-Martinez JM, Gabaldon T. trimAl: a tool for automated alignment
617 trimming in large-scale phylogenetic analyses. Bioinformatics. 2009;25(15):1972-3. doi:
618 10.1093/bioinformatics/btp348. PubMed PMID: 19505945; PubMed Central PMCID:
619 PMCPMC2712344.
620 48. Price MN, Dehal PS, Arkin AP. FastTree 2--approximately maximum-likelihood trees for large
621 alignments. PloS one. 2010;5(3):e9490. doi: 10.1371/journal.pone.0009490. PubMed PMID:
622 20224823; PubMed Central PMCID: PMCPMC2835736.
623 49. Minh BQ, Schmidt HA, Chernomor O, Schrempf D, Woodhams MD, von Haeseler A, et al. IQ-
624 TREE 2: New Models and Efficient Methods for Phylogenetic Inference in the Genomic Era. Mol Biol
625 Evol. 2020;37(5):1530-4. doi: 10.1093/molbev/msaa015. PubMed PMID: 32011700; PubMed Central
626 PMCID: PMCPMC7182206.
627 50. Hoang DT, Chernomor O, von Haeseler A, Minh BQ, Vinh LS. UFBoot2: Improving the
628 Ultrafast Bootstrap Approximation. Mol Biol Evol. 2018;35(2):518-22. doi: 10.1093/molbev/msx281.
629 PubMed PMID: 29077904; PubMed Central PMCID: PMCPMC5850222.
630 51. Gu X, Fu YX, Li WH. Maximum likelihood estimation of the heterogeneity of substitution rate
631 among nucleotide sites. Mol Biol Evol. 1995;12(4):546-57. doi:
632 10.1093/oxfordjournals.molbev.a040235. PubMed PMID: 7659011.
633 52. Kalyaanamoorthy S, Minh BQ, Wong TKF, von Haeseler A, Jermiin LS. ModelFinder: fast
634 model selection for accurate phylogenetic estimates. Nature methods. 2017;14(6):587-9. doi:
635 10.1038/nmeth.4285. PubMed PMID: 28481363; PubMed Central PMCID: PMCPMC5453245.
636 53. Sheiner L, Demerly JL, Poulsen N, Beatty WL, Lucas O, Behnke MS, et al. A systematic screen
637 to discover and analyze apicoplast proteins identifies a conserved and essential protein import
638 factor. PLoS pathogens. 2011;7(12):e1002392. doi: 10.1371/journal.ppat.1002392. PubMed PMID:
639 22144892; PubMed Central PMCID: PMCPMC3228799.
640 54. Roos DS, Donald RG, Morrissette NS, Moulton AL. Molecular tools for genetic dissection of
641 the protozoan parasite Toxoplasma gondii. Methods Cell Biol. 1994;45:27-63. doi: 10.1016/s0091-
642 679x(08)61845-2. PubMed PMID: 7707991.

643

644 **FIGURE LEGENDS**

645 Figure 1: *T. gondii* encodes homologues of cell cycle checkpoint kinases

646 Phylogeny inferred from amino acid sequences of ATR, ATM and TOR homologues from various
647 eukaryotes. The tree is rooted on PI3K and PI4K sequences, which are paralogues of ATR, ATM and
648 TOR, from Opisthokonts and Apicomplexa. Support values, displayed as percentages, were
649 generated from 1000 ultrafast bootstrap replicates [50] and only support values ≥ 95, indicating that
650 strongly supported clades are shown. Strongly supported clades are highlighted for ATR (support
651 value = 100) and ATM (support value = 99) sequences (yellow and green, respectively). The scale bar
652 represents the number of amino acid substitutions per site. A fully-expanded version of this tree
653 with no collapsed clades and displaying sequence accessions is provided in Figure S1.

654

655 Figure 2: Inducible knockdown of *Tg*ATM and *Tg*ATR

656 A,B. Constructs used for tagging the *Tg*ATM (A) and *Tg*ATR (B) genes in the *T. gondii* genome.
657 DHFR*, dihydrofolate reductase (selectable marker gene).

658 C,D. IFA showing HA-tagged *Tg*ATM (C) and *Tg*ATR (D) in intracellular tachyzoites: representative
659 cells are shown from each tagged line, before and after addition of ATc for 24 h. Scale bar, 2
660 µm.

661 E,F Quantification of IFA signals in the parental control line (Δ*ku80*:TATi), each tagged line, and
662 each knockdown (k/d, ATc treated for 24 h): *Tg*ATM (E) and *Tg*ATR (F). N = 50 parasites
663 quantified per condition. Ordinary one-way ANOVA and post hoc Tukey's multiple
664 comparisons tests of all samples; P values: *<0.05, **<0.01, ***<0.001, ****<0.0001.
665 Comparisons not shown, ns.

666

667 Figure 3: Knockdown of *Tg*ATM or *Tg*ATR imposes no growth defect or sensitivity to DNA damage

668 A,B. Images of three replicate plaque assays, either untreated (control) or treated with ATc to
669 induce *Tg*ATM k/d (A) and *Tg*ATR k/d (B).

670 C,D. Plaque assay images are shown with or without DNA damage, CPT or MMS, at the
671 concentrations stated for 10 days. *Tg*ATM k/d (C) or *Tg*ATR k/d (D) parasites were pre-
672 treated with ATc for 24 h and then additionally treated with DNA damaging agents for 10
673 days. Representative images from three biological replicates are shown.
674 E,F. The percentage area of plaques in each background of host cells was quantified from
675 representative images shown in A, B, C and D: three biological replicates were quantified for
676 each condition. Ordinary one-way ANOVA and post hoc Tukey's multiple comparisons tests
677 were made of each condition vs PIKK k/d, and control vs all; P values: *<0.05, **<0.01,
678 ***<0.001, ****<0.0001. Comparisons not shown, ns.
679
680 Figure 4: Knockdown of *Tg*ATM or *Tg*ATR ablates acute checkpoint-like responses to DNA damage
681 A Images of representative vacuoles containing 2, 4, 8 or 16 parasites, as counted for the
682 graphs in B and C after 24h growth. Scale bar 2 µm.
683 B,C. Replication assays were conducted on *Tg*ATM k/d (B) and *Tg*ATR k/d (C) parasites, grown for
684 24h under DNA-damaging conditions. Numbers of parasites in 250 vacuoles were counted
685 per condition in each experiment; data from 2-3 biological replicates are shown. Ordinary
686 one-way ANOVA and post hoc Tukey's multiple comparisons tests were made of control vs
687 all other conditions, and of each drug treatment vs k/d with the same treatment. P values:
688 *<0.05, **<0.01, ***<0.001, ****<0.0001. Comparisons not shown, ns. Also not shown on
689 the graph, for concision: the ATM control line differed from the same line under all DNA
690 damage conditions at p-value ****<0.0001; the ATR control also differed from all DNA
691 damage conditions at p-value ****<0.0001 except ***<0.001 for 2.5uM CPT.
692 D,E. IFA of H2AX phosphorylation in *Tg*ATM k/d (D) and *Tg*ATR k/d (E) tachyzoites that were
693 treated for 2 h with DNA-damaging agents. Representative images from three biological
694 replicates are shown. Scale bar 2 µm.

695 F Mean H2AX signal in nuclei was quantified from representative images in D and E using
696 ImageJ. 40 nuclei were quantified per condition for three biological replicates. Ordinary one-
697 way ANOVA and post hoc Tukey's multiple comparisons tests were performed for control vs
698 k/d and single drug treatment; and single drug treatment vs k/d plus drug; P values: *<0.05,
699 **<0.01, ***<0.001, ****<0.0001. Comparisons not shown, ns.
700
701 Figure 5: <u>*Tg*ATR does not behave quantifiably differently in the presence or absence of *Tg*ATM</u>
702 A. Construct used to tag the *TgATR* gene with V5, under the tubulin (Tub) promoter and
703 chloramphenicol resistance selectable marker (CAT). Also shown is the original construct
704 used to tag the *TgATM* gene with HA. Schematics show where PCR primers were located to
705 test correct integration of the two tags. The PCR results on the left shows V5-tagged *TgATR*
706 after transfection of this construct into the *Tg*ATM-HA line (no band appeared in the
707 parental control line ('Δ*ku80*:TATi') or in either single-gene-tagged line); the PCR on the right
708 shows that HA-tagged *TgATM* remained in the double-tagged line.
709 B. IFA showing parasites with both ATR and ATM tagged, in either control or *Tg*ATM knockdown
710 conditions, treated with DNA damaging drug treatments for 2 h, 24 h after infection of fresh
711 host cells. Scale bar, 2 µm.
712 C. Using IFA images as in (B), maximum brightness of *Tg*ATR and *Tg*ATM foci was measured in
713 both control and ATM-knockdown conditions, as well as in the parental line (Δ*ku80*:TATi).
714 One biological replicate was analysed; n = 50 parasites quantified per condition. Ordinary
715 one-way ANOVA and post hoc Tukey's multiple comparisons tests of control vs all conditions
716 for both *Tg*ATR and *Tg*ATM were completed; P values: *<0.05, **<0.01, ***<0.001,
717 ****<0.0001. Comparisons not shown, ns.
718 D. Mean brightness of *Tg*ATR and *Tg*ATM signals throughout parasites, measured in both
719 control and ATM-knockdown conditions, as well as the parental line (Δ*ku80*:TATi). N = 50
720 parasites quantified per condition. Statistical analysis as in (C).

721 E,F. Using IFA images as in (B), the amount of signal in the nucleus and in the whole cell
722 was quantified for both *Tg*ATR (E) and *Tg*ATM (F), with or without ATM k/d and addition of
723 50µM CPT or 500µM MMS. One biological replicate was analysed in this experiment; n = 50
724 parasites per condition. Ordinary one-way ANOVA and post hoc Tukey's multiple
725 comparisons tests of control vs all conditions for both *Tg*ATR and *Tg*ATM were completed; P
726 values: *<0.05, **<0.01, ***<0.001, ****<0.0001. Comparisons not shown, ns.
727

728 Figure 6: <u>KU-55933, an inhibitor of human ATM, does not phenocopy knockdown of *Tg*ATM or</u>
729 <u>*Tg*ATR</u>

730 A. Images of plaque assays conducted in the *Tg*ATM and *Tg*ATR HA-tagged lines treated with
731 increasing concentrations of KU-55933.
732 B. Images of plaque assays showing the same lines as in (A), treated with KU-55933, after
733 knockdown of *Tg*ATM or *Tg*ATR.
734 C. The percentage area of plaques in each background of host cells was quantified from
735 representative images shown in A and B: three biological replicates were quantified for each
736 condition. Ordinary one-way ANOVA and post hoc Tukey's multiple comparisons tests were
737 made of control vs all, KU-55933 treatments against each other, and KU-55933 treatment at
738 2.5µM with vz without PIKK k/d. P values: *<0.05, **<0.01, ***<0.001, ****<0.0001.
739 Comparisons not shown, ns.
740 D. Using IFA images, the maximum brightness of *Tg*ATR and *Tg*ATM foci was measured in both
741 control and ATM-knockdown conditions, with or without KU-55933. One biological replicate
742 was analysed; n = 50 parasites quantified per condition. Ordinary one-way ANOVA and post
743 hoc Tukey's multiple comparisons tests of control vs all conditions for both *Tg*ATR and
744 *Tg*ATM were completed; P values: *<0.05, **<0.01, ***<0.001, ****<0.0001. Comparisons
745 not shown, ns.

746 E. Mean brightness of *Tg*ATR and *Tg*ATM signals throughout parasites, measured in both
747 control and ATM-knockdown conditions, with or without KU55933. N = 50 parasites
748 quantified per condition. Statistical analysis as in (D).
749 F. IFA showing H2AX foci in the parental strain, treated or not treated with KU55933, with or
750 without DNA-damaging drugs MMS or CPT. Scale bar, 2 µm. Mean H2AX signals were then
751 quantified in 40 nuclei per condition, from three biological replicates, and these are shown
752 in the graph (control data are shown alongside, as in Figure 4). Ordinary one-way ANOVA
753 and post hoc Tukey's multiple comparisons tests were made; P values: *<0.05, **<0.01,
754 ***<0.001, ****<0.0001. Comparisons not shown, ns.

755

756 **SUPPLEMENTARY FIGURE LEGENDS**

757 Figure S1: Homologues of cell cycle checkpoint kinases in Apicomplexans and other eukaryotes

758 A fully expanded version of the phylogenetic tree shown in Figure 1.

759

760 Figure S2: Inducible knockdown of *Tg*ATM and *Tg*ATR

761 *A.* The phenotype score for *Tg*ATM from a genome-wide CRISPR screen to identify essential
762 genes in *T. gondii* (Sidik et al., 2016).
763 *B.* The phenotype score for *Tg*ATR from a genome-wide CRISPR screen to identify essential
764 genes in *T. gondii* (Sidik et al., 2016).
765 *C.* The schematic shows where the primers were located for PCR-based testing of correct
766 integration of the HA tag on the *ATM* gene. The PCR shows the correct size band was
767 present in all ATM clones and not in the parental control line. Asterisks denote non-specific
768 bands that amplified from both the parental line ('Δ*ku80*:TATi') and HA-tagged clones.

769 *D.* The schematic shows primers designed to test for correct integration of the HA tag on the
770 *ATR* gene. The PCR shows correct integration in several clones and the absence of a product
771 from the parental control line; an HA-tagged ATM control (as in C) is also shown.
772 *E.* Anti-HA western blot of samples from an ATM tagged clone, taken at 24, 48 and 72 h after
773 the addition of ATc. Profilin was used as a control protein.
774
775 Figure S3: ATc has no effect on the DNA damage checkpoint response of the host cell of *T. gondii,*
776 whereas KU-55933 inhibits this response.

777 Immunofluorescence images showing that phosphorylation of H2AX in the host cell nucleus a) was
778 not affected by addition of ATc, in cells either uninfected or infected with the parental line of *T.*
779 *gondii*, Δ*ku80*:TATi; b) was inhibited upon addition of the KU-55933 inhibitor. Cells were treated
780 with 0.5mg/ml ATc, 50 μM CPT, 50μM KU-55933, or combinations of these. Representative images
781 from one biological replicate are shown. Scale bar 5 μm.
782
783 Figure S4: Resource table

784 *A.* Table containing plasmid maps.
785 *B.* Table containing protospacer and primer sequences.
786 *C.* Table containing antibodies used.
787

Figure 1:

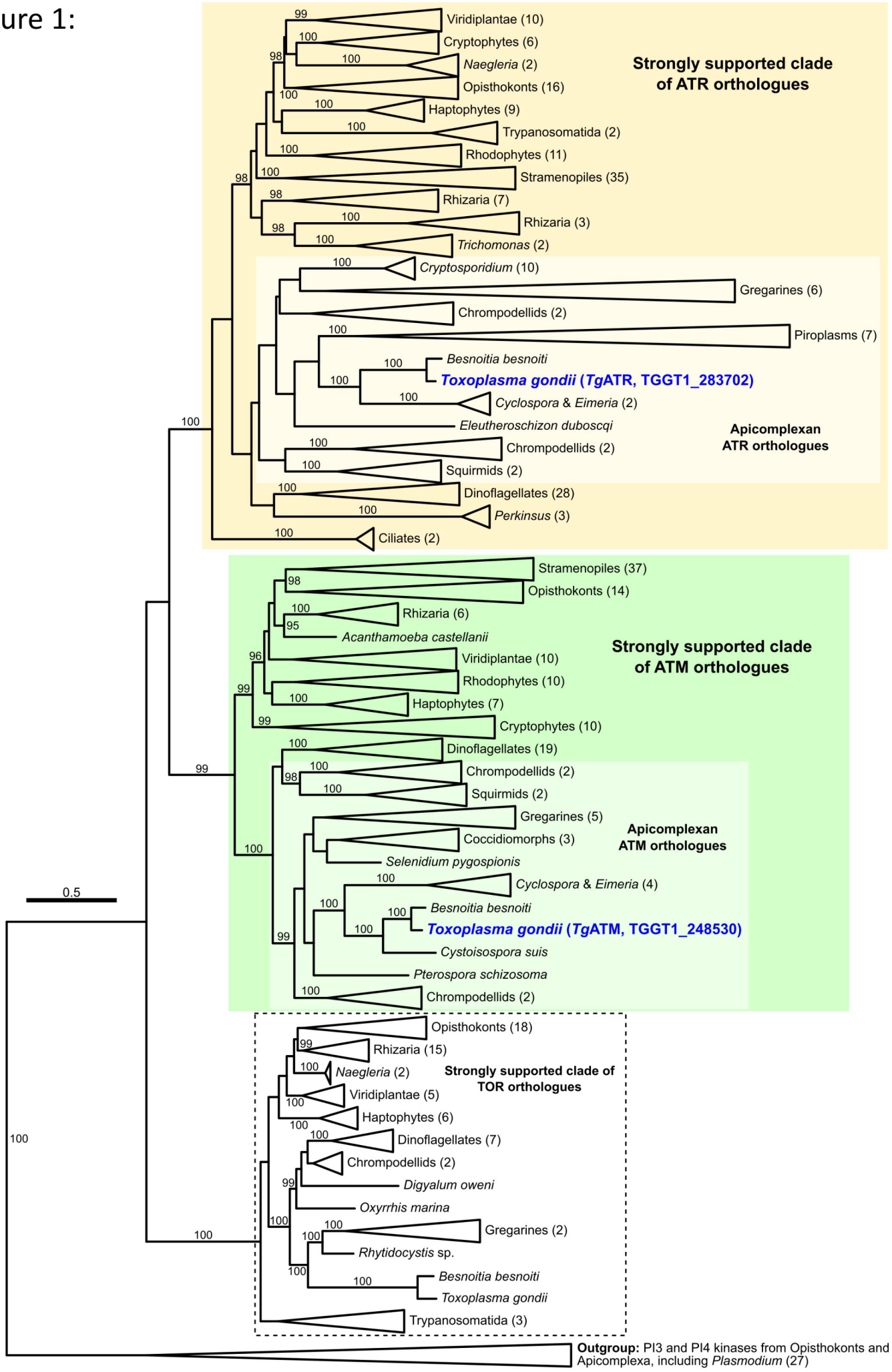
Strongly supported clade of ATR orthologues
Viridiplantae (10)
Cryptophytes (6)
Naegleria (2)
Opisthokonts (16)
Haptophytes (9)
Trypanosomatida (2)
Rhodophytes (11)
Stramenopiles (35)
Rhizaria (7)
Rhizaria (3)
Trichomonas (2)
Cryptosporidium (10)
Gregarines (6)
Chrompodellids (2)
Piroplasms (7)
Besnoitia besnoiti
Toxoplasma gondii (TgATR, TGGT1_283702)
Cyclospora & Eimeria (2)
Eleutheroschizon duboscqi
Apicomplexan ATR orthologues
Chrompodellids (2)
Squirmids (2)
Dinoflagellates (28)
Perkinsus (3)
Ciliates (2)
Strongly supported clade of ATM orthologues
Stramenopiles (37)
Opisthokonts (14)
Rhizaria (6)
Acanthamoeba castellanii
Viridiplantae (10)
Rhodophytes (10)
Haptophytes (7)
Cryptophytes (10)
Dinoflagellates (19)
Chrompodellids (2)
Squirmids (2)
Gregarines (5)
Coccidiomorphs (3)
Selenidium pygospionis
Apicomplexan ATM orthologues
Cyclospora & Eimeria (4)
Besnoitia besnoiti
Toxoplasma gondii (TgATM, TGGT1_248530)
Cystoisospora suis
Pterospora schizosoma
Chrompodellids (2)
Strongly supported clade of TOR orthologues
Opisthokonts (18)
Rhizaria (15)
Naegleria (2)
Viridiplantae (5)
Haptophytes (6)
Dinoflagellates (7)
Chrompodellids (2)
Digyalum oweni
Oxyrrhis marina
Gregarines (2)
Rhytidocystis sp.
Besnoitia besnoiti
Toxoplasma gondii
Trypanosomatida (3)
0.5
Outgroup: PI3 and PI4 kinases from Opisthokonts and Apicomplexa, including Plasmodium (27)

Figure 2:

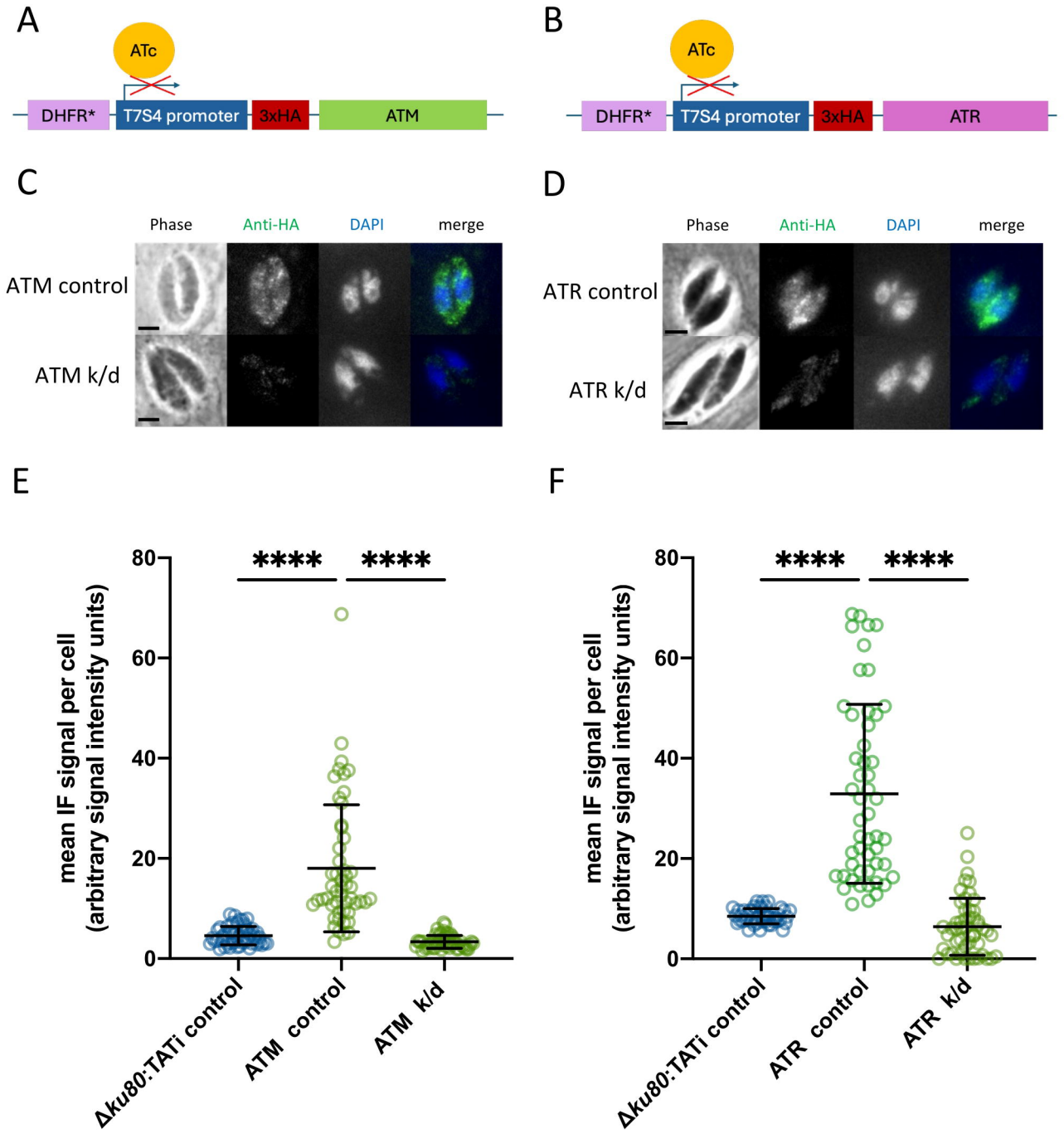
A
ATc
DHFR*
T7S4 promoter
3xHA
ATM
B
ATc
DHFR*
T7S4 promoter
3xHA
ATR
C
Phase
Anti-HA
DAPI
merge
ATM control
ATM k/d
D
Phase
Anti-HA
DAPI
merge
ATR control
ATR k/d
E
mean IF signal per cell
(arbitrary signal intensity units)
80
60
40
20
0
****
****
Δku80:TATi control
ATM control
ATM k/d
F
mean IF signal per cell
(arbitrary signal intensity units)
80
60
40
20
0
****
****
Δku80:TATi control
ATR control
ATR k/d

Figure 3:

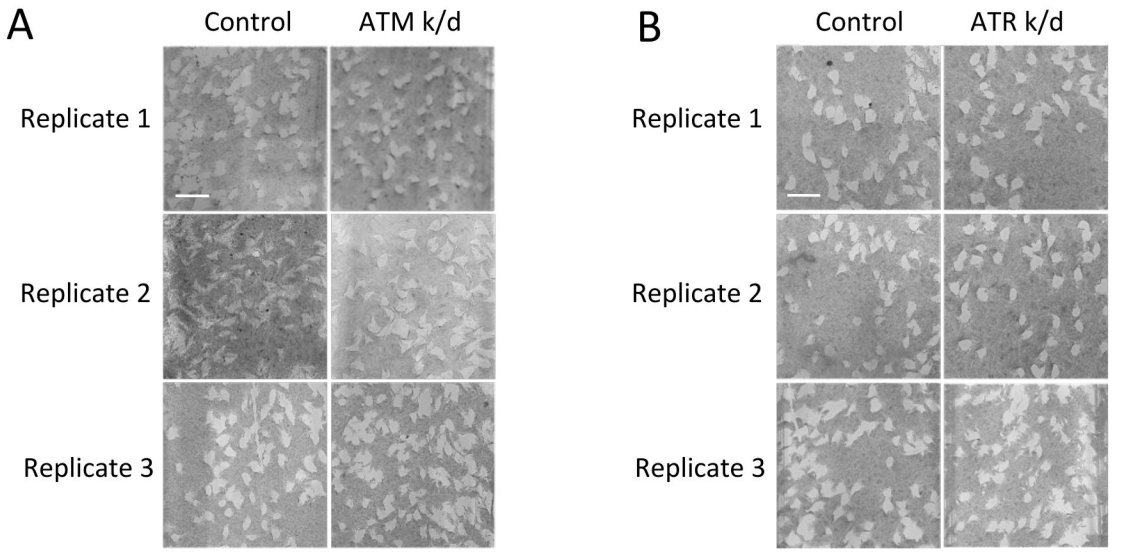
A
Control
ATM k/d
Replicate 1
Replicate 2
Replicate 3
B
Control
ATR k/d
Replicate 1
Replicate 2
Replicate 3

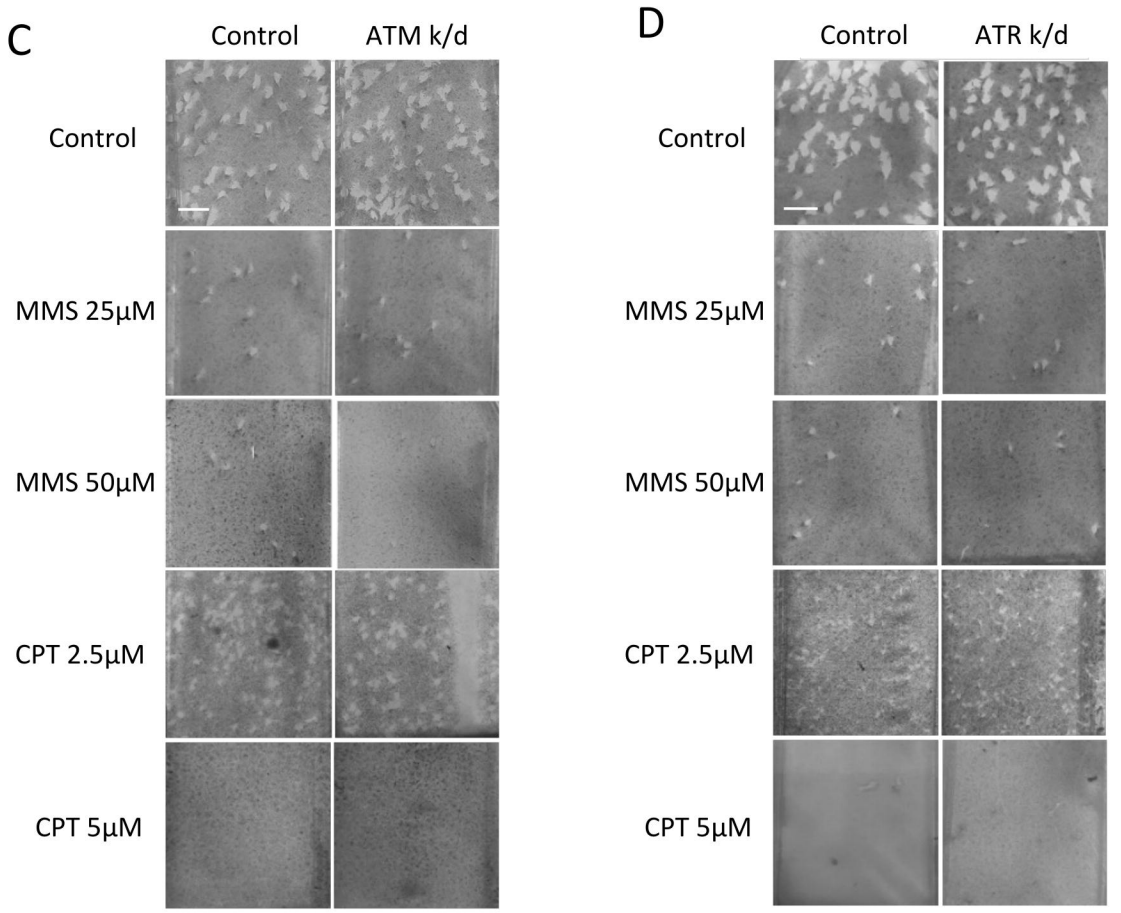
C
Control
ATM k/d
Control
MMS 25µM
MMS 50µM
CPT 2.5µM
CPT 5µM
D
Control
ATR k/d
Control
MMS 25µM
MMS 50µM
CPT 2.5µM
CPT 5µM

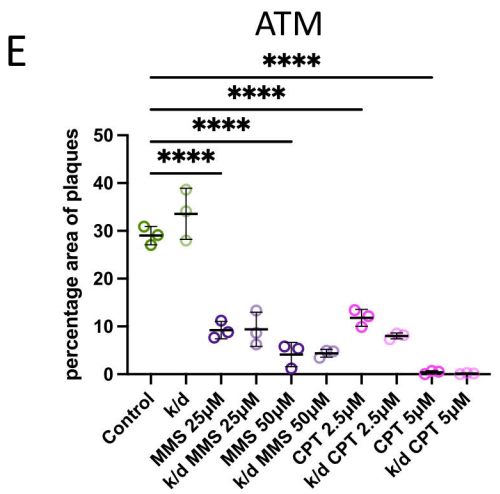
E
ATM
****
****
****
****
percentage area of plaques
50
40
30
20
10
0
Control
k/d
MMS 25µM
k/d MMS 25µM
MMS 50µM
k/d MMS 50µM
CPT 2.5µM
k/d CPT 2.5µM
CPT 5µM
k/d CPT 5µM

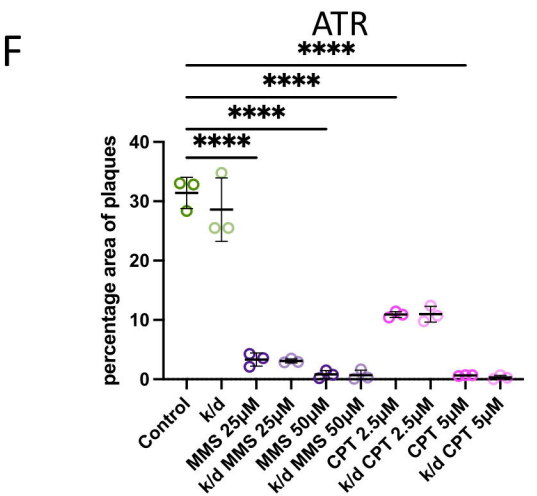
F
ATR
****
****
****
****
percentage area of plaques
40
30
20
10
0
Control
k/d
MMS 25µM
k/d MMS 25µM
MMS 50µM
k/d MMS 50µM
CPT 2.5µM
k/d CPT 2.5µM
CPT 5µM
k/d CPT 5µM

Figure 4:

A

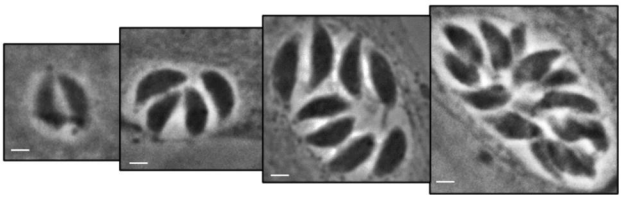

B

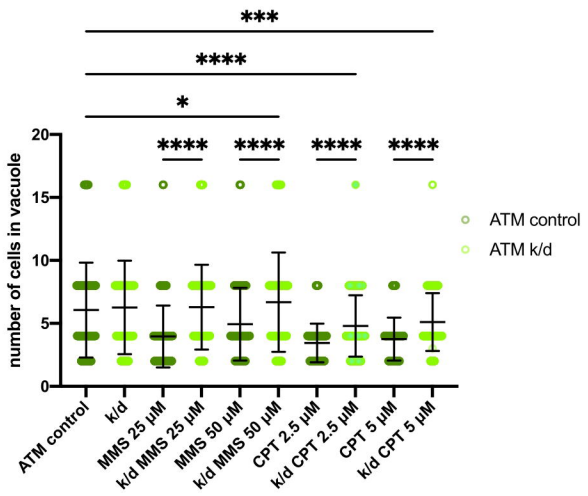

C

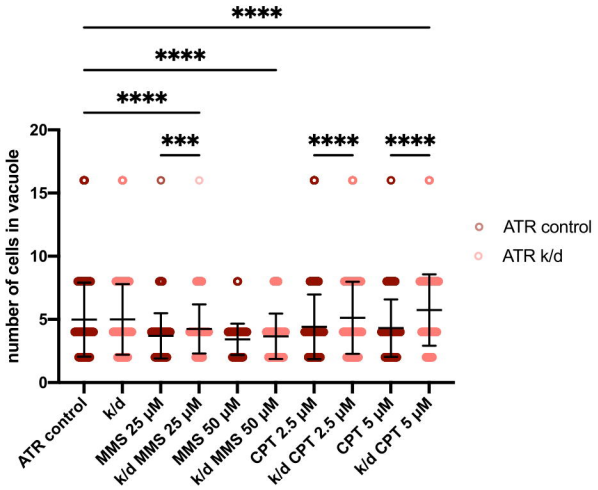

D

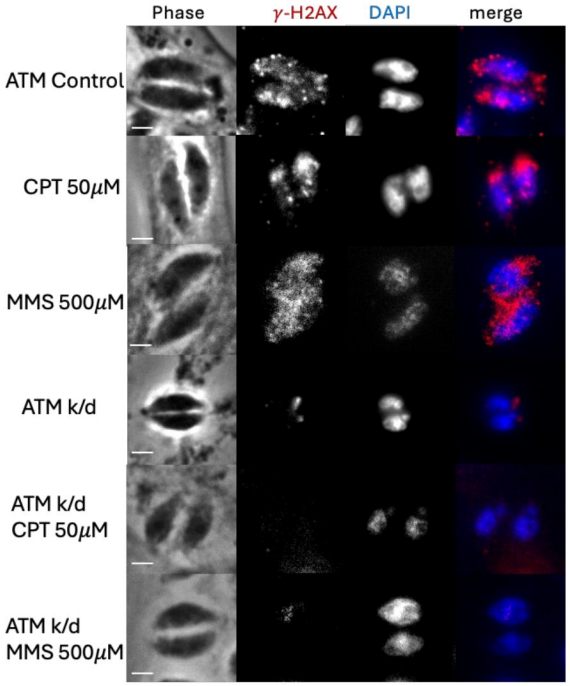

E

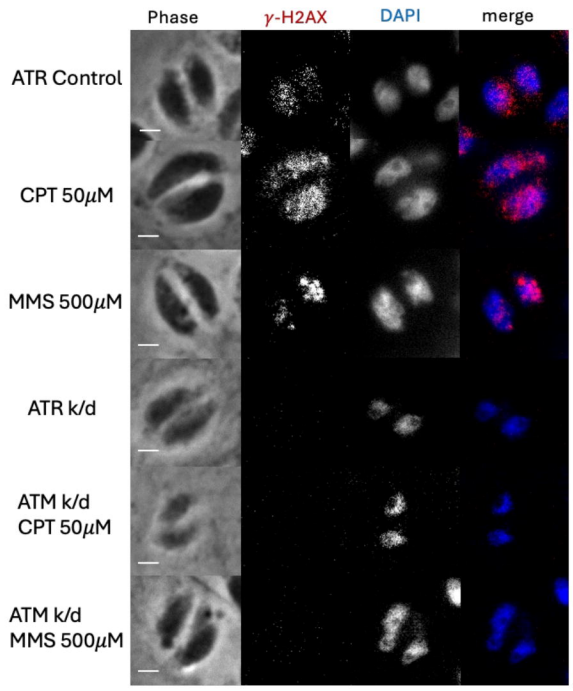

F

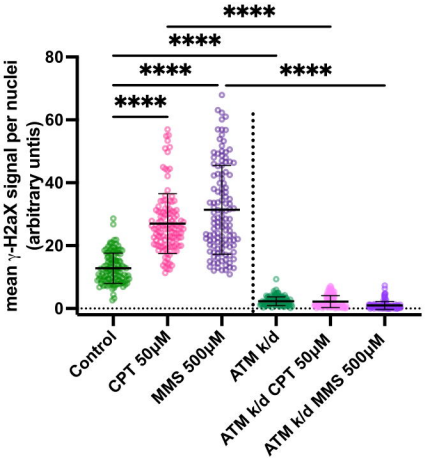

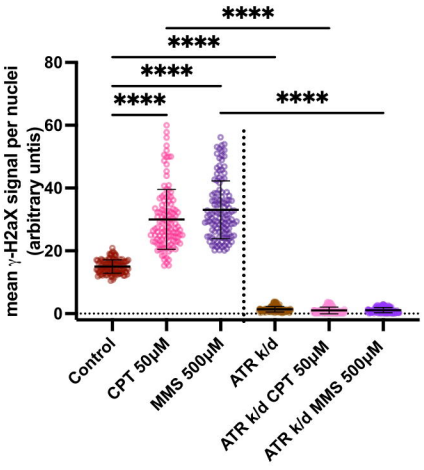

Figure 5:

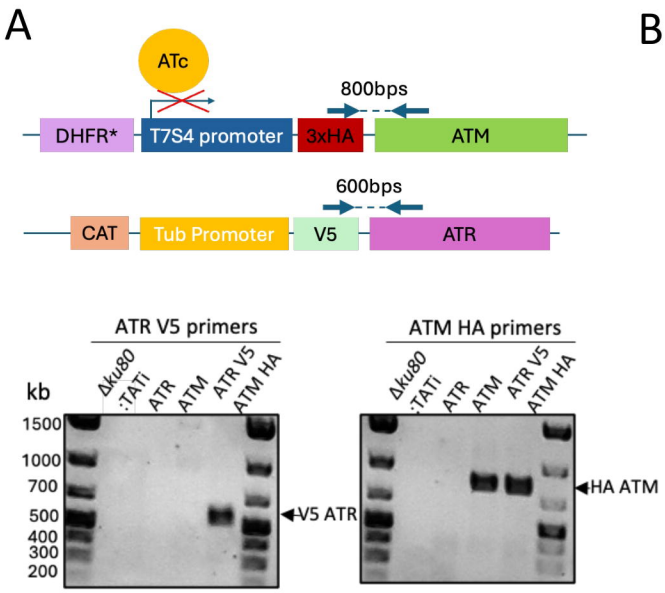
A
ATc
800bps
DHFR*
T7S4 promoter
3xHA
ATM
600bps
CAT
Tub Promoter
V5
ATR
ATR V5 primers
ATM HA primers
kb
Δku80 :TATi
ATR
ATM
ATR V5
ATM HA
1500
1000
700
500
400
300
200
V5 ATR
HA ATM

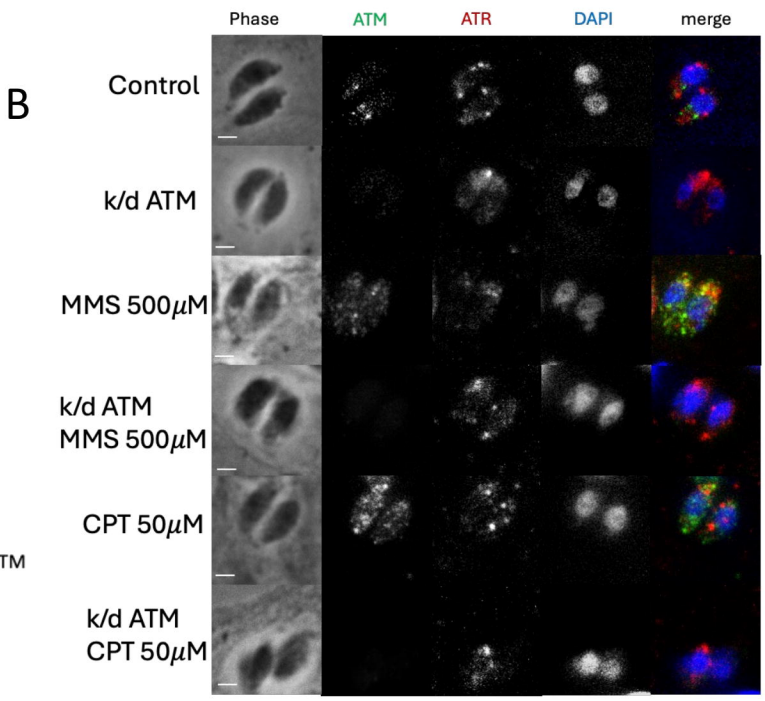
B
Phase
ATM
ATR
DAPI
merge
Control
k/d ATM
MMS 500μM
k/d ATM MMS 500μM
CPT 50μM
k/d ATM CPT 50μM

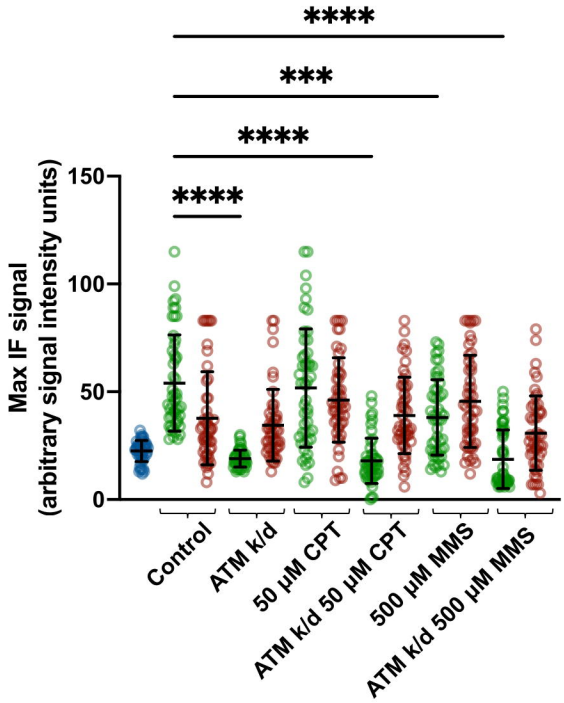
C
****
***
****
****
Max IF signal (arbitrary signal intensity units)
150
100
50
0
Control
ATM k/d
50 μM CPT
ATM k/d 50 μM CPT
500 μM MMS
ATM k/d 500 μM MMS

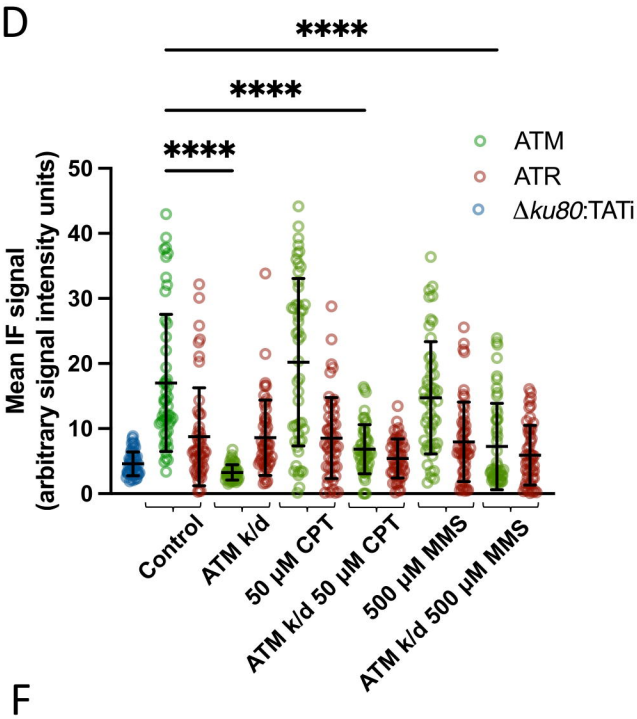
D
****
****
****
ATM
ATR
Δku80:TATi
Mean IF signal (arbitrary signal intensity units)
50
40
30
20
10
0
Control
ATM k/d
50 μM CPT
ATM k/d 50 μM CPT
500 μM MMS
ATM k/d 500 μM MMS

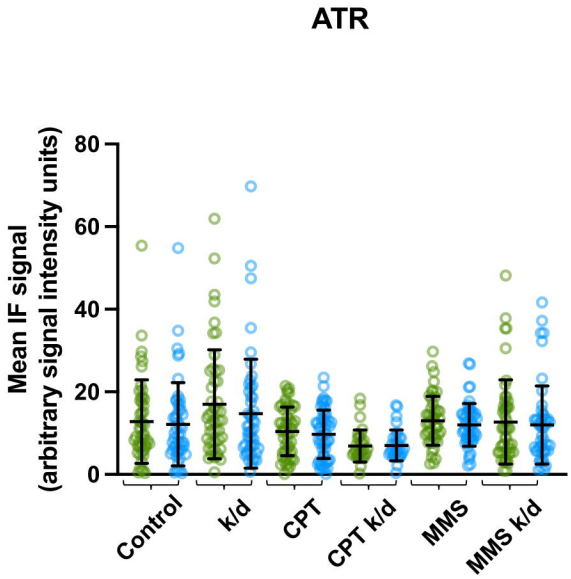
E
ATR
Mean IF signal (arbitrary signal intensity units)
80
60
40
20
0
Control
k/d
CPT
CPT k/d
MMS
MMS k/d

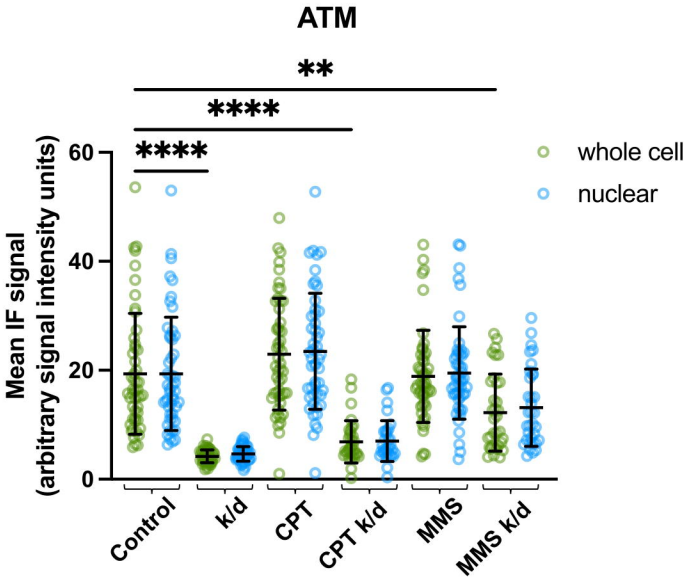
F
ATM
**
****
****
whole cell
nuclear
Mean IF signal (arbitrary signal intensity units)
60
40
20
0
Control
k/d
CPT
CPT k/d
MMS
MMS k/d

Figure 6:

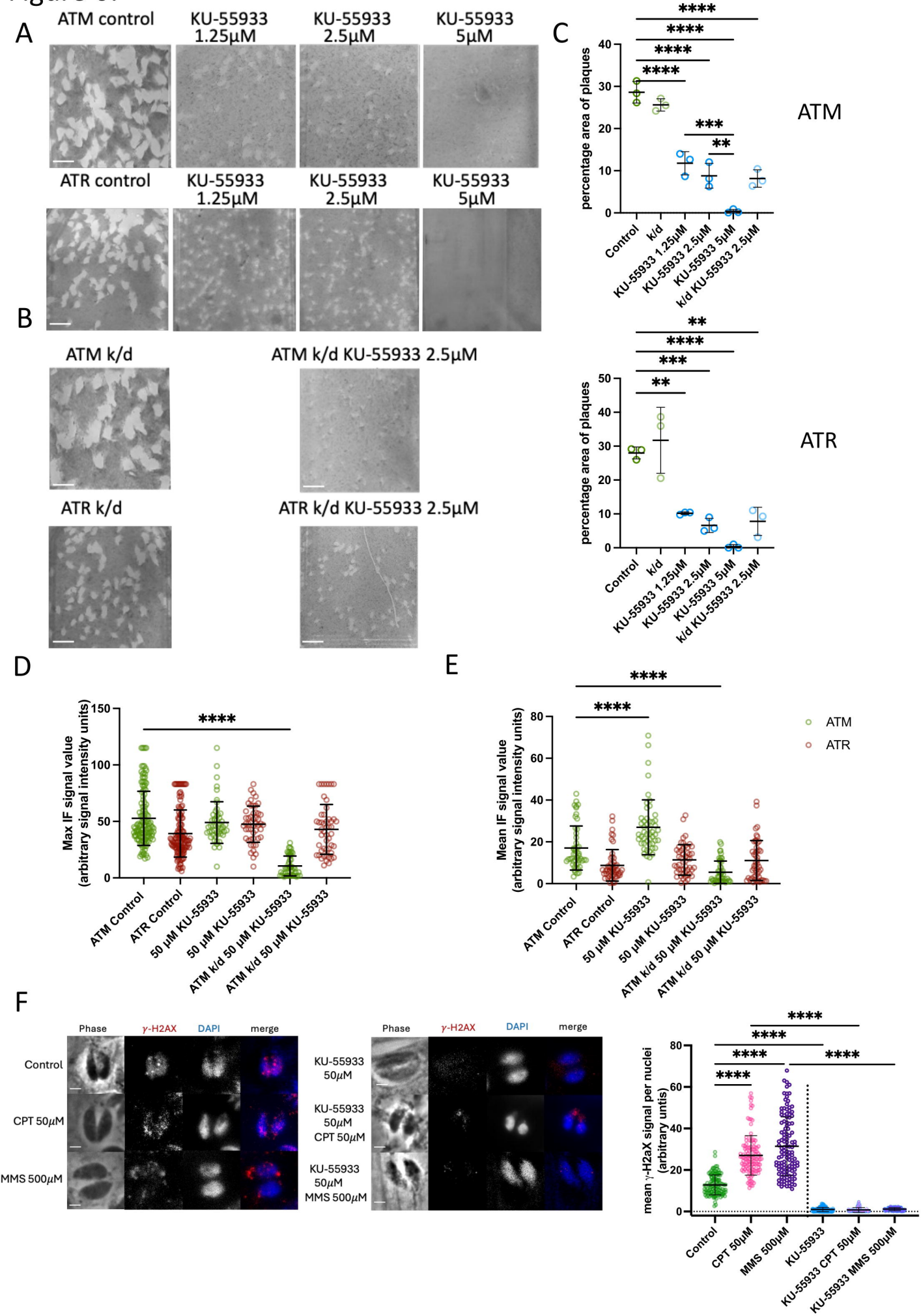
A
ATM control
KU-55933 1.25μM
KU-55933 2.5μM
KU-55933 5μM
ATR control
KU-55933 1.25μM
KU-55933 2.5μM
KU-55933 5μM
B
ATM k/d
ATM k/d KU-55933 2.5μM
ATR k/d
ATR k/d KU-55933 2.5μM
C
ATM
percentage area of plaques
Control
k/d
KU-55933 1.25μM
KU-55933 2.5μM
KU-55933 5μM
k/d KU-55933 2.5μM
ATR
D
Max IF signal value (arbitrary signal intensity units)
ATM Control
ATR Control
50 μM KU-55933
ATM k/d 50 μM KU-55933
E
Mean IF signal value (arbitrary signal intensity units)
ATM
ATR
F
Phase
γ-H2AX
DAPI
merge
Control
CPT 50μM
MMS 500μM
KU-55933 50μM
KU-55933 50μM CPT 50μM
KU-55933 50μM MMS 500μM
mean γ-H2aX signal per nuclei (arbitrary untis)
CPT 50μM
MMS 500μM
KU-55933
KU-55933 CPT 50μM
KU-55933 MMS 500μM